XCTFormer: Leveraging Cross-Channel and Cross-Time Dependencies for Enhanced Time-Series Analysis

Anonymous authors
Paper under double-blind review

Abstract

Multivariate time-series analysis involves extracting informative representations from sequences of multiple interdependent variables, supporting tasks such as forecasting, imputation, and anomaly detection. In real-world scenarios, these variables are typically collected from a shared context or underlying phenomenon, which suggests the presence of latent dependencies across both time and channels that can be leveraged to improve performance. However, recent findings have shown that channel-independent (CI) models, which assume no inter-variable dependencies, often outperform channel-dependent (CD) models that explicitly attempt to model such relationships. This surprising result indicates that current CD models may not fully exploit their potential due to limitations in how dependencies are captured. Recent studies have revisited channel dependence modeling with various approaches; however, these methods often employ indirect modeling strategies, which can lead to potential information loss. To address this issue, we introduce **XCTFormer**, a transformer-based channel-dependent (CD) model that explicitly captures cross-temporal and cross-channel dependencies via an enhanced attention mechanism. The model operates in a *token-to-token* fashion, modeling pairwise dependencies between every pair of tokens across time and channels. The architecture comprises (i) a data processing module, (ii) a novel Cross-Relational Attention Block (CRAB) that increases capacity and expressiveness, and (iii) an optional Dependency Compression Plugin (DeCoP) that improves scalability. Through extensive experiments on three time-series benchmarks, we show that **XCTFormer** achieves superior results compared to widely recognized baselines; in particular, it attains state-of-the-art performance on the imputation task, outperforming the second-best method by an average of 24.1% in MSE and 17.6% in MAE.

1 Introduction

Forecasting, anomaly detection, and imputation are critical tasks in various real-world domains, with a wide range of applications (Jin et al., 2024). For instance, forecasting is utilized in energy management, weather prediction, healthcare, and more (Mystakidis et al., 2024; Brunet et al., 2023; Duarte et al., 2021). Time-series analysis plays a vital role in extracting key information from sequential data to facilitate these tasks. The effectiveness of this information extraction is crucial, as it directly impacts the performance of subsequent time-series tasks (Trirat et al., 2024). Accurate time-series analysis enables organizations to enhance decision-making and optimize resource allocation (Bui et al., 2018; Wang et al., 2024b), highlighting the importance of the information extraction component as a key area of research.

Time-series data can be modeled using two main approaches (Han et al., 2024). Univariate approaches treat each channel independently, disregarding any potential relationships between them. In contrast, *multivariate* approaches take into account not only the temporal behavior within each channel but also the possible dependencies among different channels. In real-world scenarios, multivariate datasets are often derived from a common underlying process or phenomenon, which typically leads to dependencies among the features (Chen et al., 2024). Incorporating relevant signals enhances representation quality and improves accuracy in downstream tasks (Isik et al., 2025; Domingos, 2012). As a result, multivariate models are generally expected to outperform univariate models by leveraging both cross-channel dependencies and

temporal dynamics. Therefore, time-series analysis can benefit significantly from richer representations when cross-channel dependencies are utilized.

However, recent work in time-series forecasting by Han et al. (2024) challenged this assumption by showing that channel-independent (CI) models, which treat multivariate time-series as separate univariate channels and ignore potential inter-channel correlations, outperform channel-dependent (CD) models that explicitly model such dependencies. They attribute this surprising outcome to a trade-off between capacity, defined as a model's ability to fit complex patterns, and robustness, defined as its ability to remain accurate under noise, input variation, or distribution shifts. While CD models gain capacity by incorporating cross-channel information, this often comes at the expense of robustness, making them more sensitive to distribution shifts. In contrast, CI models sacrifice some capacity by ignoring cross-channel dependencies, resulting in enhanced robustness and improved generalization accuracy. These findings challenge the common belief that adding relevant information usually leads to better representation quality and accuracy, revealing a gap between channel-dependent methods and their unrealized potential. Motivated by these findings, we seek in this paper to address the following question:

> *How should we model sequential cross-channel information to realize its potential?*

Recent research has revisited channel dependence with cross-channel modeling approaches that often outperform channel-independent (CI) baselines. iTransformer (Liu et al., 2024) targets cross-channel dependencies by treating each channel as a token and applying a Transformer on the token sequence. CrossFormer (Zhang & Yan, 2023) and CARD (Wang et al., 2024c) address both cross-channel and cross-time relationships, but they employ a two-stage pipeline for sequence modeling and channel processing, which can lead to information loss at the stage interfaces. Despite recent advancements, most methods only model dependencies across different channels and time *indirectly*, which can lead to significant interactions being overlooked. Additionally, cross-channel dependencies are often unknown in advance, as the underlying generative process is typically unknown. These dependencies may also change over time (Zhao & Shen, 2024), raising the need for simultaneous cross-channel cross-time modeling. To address these challenges, we propose a *direct* modeling strategy with a *token-to-token* approach that explicitly captures each token's pairwise dependencies across all channels and time-steps. This potentially minimizes essential information loss associated with existing indirect models. To accomplish this, we introduce **XCTFormer**, a Transformer-based framework that models directly all possible dependencies within a single attention block, modeling them token-to-token and effectively identifying the most relevant dependencies for downstream tasks.

The backbone of the **XCTFormer** consists of three novel components: (i) data processing unit, (ii) the Cross-Relational Attention Block (CRAB), and (iii) the Dependency Compression Plugin (DeCoP). First, we independently patch each channel and tokenize the data. Next, we flatten the channel and time dimensions, which allows CRAB and DeCoP to capture all possible dependencies in a token-to-token manner. CRAB represents an enhancement of the standard attention block (Vaswani et al., 2017) with two key modifications aimed at improving expressivity and robustness. First, it introduces a learnable, non-boolean masking mechanism that supplements conventional binary masks by weighting dependencies according to their learned importance. This allows the model to focus on the most crucial dependencies for the downstream task. Second, CRAB replaces the standard softmax function with a new normalization technique that retains the necessary properties required for attention activation (Saratchandran et al., 2025) while permitting negative weights. This extension increases the expressiveness of the model by enabling it to capture a wider array of relationships, as suggested by Lv et al. (2024). Lastly, DeCoP is an optional plugin for CRAB aimed at enhancing scalability for datasets with numerous channels. It addresses the memory limitations imposed by the transformer's quadratic attention mechanism. DeCoP compresses the quadratic attention into a linear form while minimizing information loss through a learnable compression transformation. We evaluated XCTFormer against various baseline models on multiple downstream tasks including forecasting, anomaly detection, and imputation, demonstrating superior results. Our main contributions are:

1. We identify a key limitation in the current literature on time-series modeling: while analysis methods have advanced substantially, little emphasis has been placed on explicitly capturing both cross-channel and cross-time dependencies in a unified manner. Most existing approaches either model temporal

      patterns or inter-channel relations separately, which restricts their ability to exploit the full structure of multivariate time-series data.

2. To address this gap, we propose XCTFormer, a general-purpose framework that models all cross-channel and cross-time dependencies directly through token-to-token mappings. XCTFormer integrates two complementary components: (i) CRAB, which enhances expressiveness by learning importance-aware attention masks and allowing signed attention activations, and (ii) DeCoP, which mitigates scalability bottlenecks on high-dimensional data through learnable compression without significant information loss.

3. We validate our approach across three fundamental time-series tasks: forecasting, anomaly detection, and imputation, achieving consistent and substantial improvements over state-of-the-art (SoTA) baselines. In particular, our method yields average error reductions of 24.1% in MSE and 17.6% in MAE for imputation, alongside notable gains in forecasting accuracy and anomaly detection robustness.

2 Related Work

From Classical Methods to Deep Architectures. Multivariate time-series analysis has progressed from traditional statistical models like ARIMA (Box & Jenkins, 1970), which often struggle to capture nonlinear dynamics, to deep neural approaches such as LSTM (Hochreiter & Schmidhuber, 1997) and TCN (Franceschi et al., 2019). While these deep models improve expressiveness, they may still fall short in modeling very long-range dependencies. More recently, time-series tasks have utilized both simple MLP-based architectures (Zeng et al., 2023; Wang et al., 2024a; Nochumsohn et al., 2025) and Transformer-based models (Zhou et al., 2021; Nie et al., 2023; Liu et al., 2024; Zhang & Yan, 2023; Wang et al., 2024c). Broadly, these models adopt either a channel-independent (CI) strategy, treating each variable separately, or a channel-dependent (CD) approach that explicitly leverages cross-variable structure.

Early CD designs: temporal focus with implicit cross-channel modeling. Early CD models emphasized efficient temporal modeling and attention computation. These methods implicitly incorporated cross-channel information by generating tokens representing all channels at the same or nearby time-steps, typically using 1D convolutions, before applying cross-time attention (Li et al., 2019b; Zhou et al., 2021; Wu et al., 2021; Liu et al., 2022b; Zhou et al., 2022). However, since inter-channel relationships were not explicitly embedded, these approaches failed to fully leverage cross-channel dependencies (Zhang & Yan, 2023). Consequently, the attention mechanism struggled to recover missing structure, leading to suboptimal representations (Liu et al., 2024).

CI baselines and channel as token formulations. On the CI side, PatchTST partitions each channel into overlapping time patches, treating these patches as tokens. These channel tokens are then passed to a stacked transformer architecture that exclusively models cross-time dependencies (Nie et al., 2023). Linear models, when applied independently to each channel, have also demonstrated competitive performance (Zeng et al., 2023; Das et al., 2023). MTLinear (Nochumsohn et al., 2025) is CI: it first clusters channels and then trains a predictor for each cluster to mitigate multi-task objective conflicts, but cross-channel dependencies are not modeled explicitly. To reintroduce cross-channel interactions, iTransformer represents each entire channel as a single token, enabling self-attention to operate across variables (Liu et al., 2024). LEDDAM (Yu et al., 2024) takes a different approach by decomposing each series into trend and seasonal components, processing the seasonal part via parallel cross-channel and cross-time pathways before combining them. However, it still lacks a unified mechanism that jointly models both dimensions within its attention module.

Two-stage explicit cross-time and cross-channel modeling. CrossFormer addresses the limitations of earlier models by dividing each channel into equal-length segments and embedding these segments individually to better preserve semantic information (Zhang & Yan, 2023). This approach, along with CARD (Wang et al., 2024c), utilizes a two-stage attention scheme: first attending along the temporal dimension, then explicitly across channels. While this sequential treatment is effective, it captures cross-channel temporal dependencies only *indirectly*, which may result in information loss and limited expressiveness.

3 Vanilla Transformer Attention

To facilitate a clear understanding of our proposed modifications, we first outline the standard transformer attention mechanism (Vaswani et al., 2017). Considering an input sequence $X \in \mathbb{R}^{N \times D_i}$, where N denotes the sequence length and D_i the per-token input feature dimension. In our case, the same sequence serves to form queries, keys, and values. The attention block projects X with learnable matrices (with D_m being the per-head attention dimension):

$$W_q, W_k, W_v \in \mathbb{R}^{D_i \times D_m}, \qquad Q = XW_q, \ K = XW_k, \ V = XW_v, \quad Q, K, V \in \mathbb{R}^{N \times D_m}.$$

Scaled dot-product scores quantify pairwise query–key affinity:

$$A = \frac{QK^\top}{\sqrt{D_m}} \in \mathbb{R}^{N \times N}.$$

An optional mask $M \in \mathbb{R}^{N \times N}$ encodes disallowed positions (e.g., padding or future time-steps) via

$$M_{ij} = \begin{cases} 0, & \text{allowed} \\ -\infty, & \text{blocked} \end{cases}$$

We then convert scores into attention weights row-wise and aggregate values accordingly:

$$W = \text{Softmax}(A + M) \in \mathbb{R}^{N \times N}, \qquad O = WV \in \mathbb{R}^{N \times D_m}.$$

Before normalization, the optional mask M is added to the score matrix A. Applying a row-wise softmax to $A + M$ assigns effectively zero weight to blocked entries; hence, the mask functions as a selection mechanism that suppresses specific relationships (e.g., to prevent information leakage from future time-steps). The resulting attention matrix W is nonnegative with each row summing to one, yielding a probability-like distribution over keys for each query. Consequently, the output O is a row-wise weighted combination of the value vectors governed by these attention weights, representing the output of the attention block.

4 XCTFormer

To model all pairwise dependencies while minimizing potential information loss through *direct token-to-token* modeling, we present **XCTFormer**, a Transformer-based, general-purpose, encoder-only time-series model. XCTFormer comprises a universal backbone and a task-specific head. The backbone has three components: (i) a data-processing unit, (ii) a Cross-Relational Attention Block (CRAB), and (iii) a Dependency Compression Plugin (DeCoP). Figure 1 summarizes the pipeline: panel A tokenizes the input and flattens across channels and patches to form a unified sequence that exposes all pairwise dependencies to the Transformer; panel B applies a stack of our modified Transformer equipped with CRAB (Sec. 4.2) and the optional DeCoP module (Sec. 4.3); panel C maps the resulting representations to predictions via a task-specific head.

4.1 Data Processing

To effectively capture the diverse and unknown dependency structures present in multivariate time-series, XCTFormer is designed to explicitly model all possible cross-channel and cross-temporal relationships. For each token, we define potential pairwise dependencies across channels and time points throughout the entire time series. These dependencies can take one of four potential forms: (i) self-lag relationships, where past values of the same channel may influence future states; (ii) cross-channel synchronous relationships, where channels at identical time points may influence one another; (iii) cross-channel lagged relationships, where other channels may exert temporal influence through their historical values; and (iv) forward-in-time relationships, where current values may influence subsequent values within the same or different channels. For visual representation of these dependencies, see Figure 2.
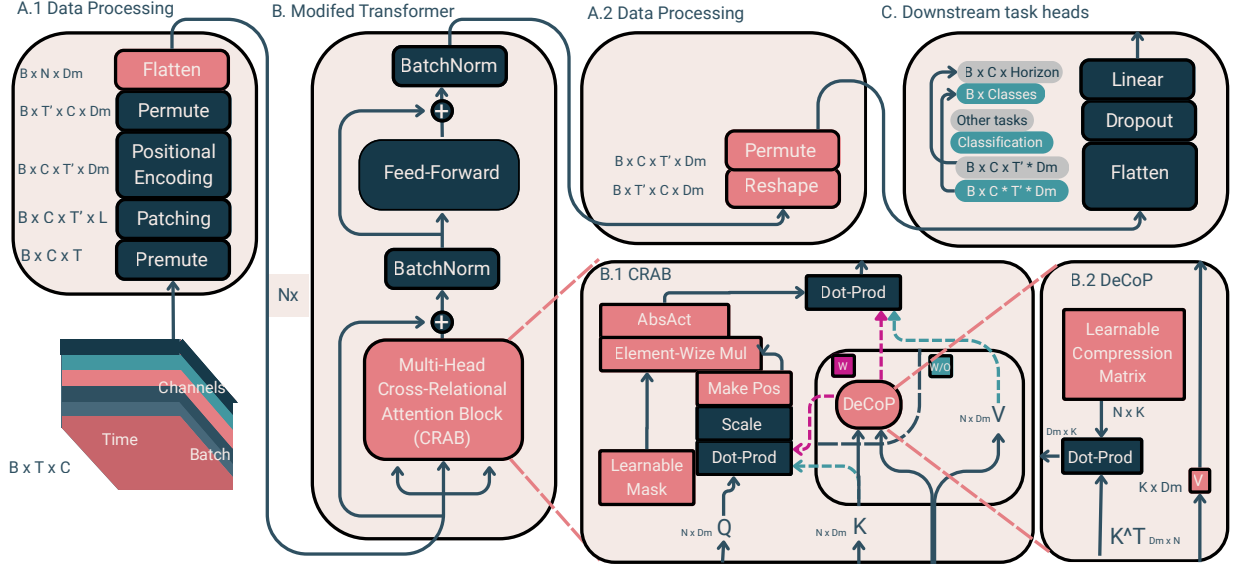
Figure 1: XCTFormer model overview. Multivariate inputs are divided into patches per channel, tokenized, and then passed as a flattened time-and-channel sequence through stacked Transformers with CRAB attention. CRAB utilizes a learnable mask and a signed, non-softmax normalization to model direct token-to-token dependencies. The optional DeCoP plugin enhances scalability by compressing pairwise attention into a compact representation, reducing memory and compute requirements. In the diagram, the pink flow represents operation with DeCoP enabled; otherwise, the blue flow is used.

Modeling dependencies at the level of individual measurements is both computationally expensive and impractical, as single measurements lack meaning without temporal context (Zeng et al., 2023). To address this, we adopt a patching strategy (Nie et al., 2023), segmenting each channel independently into short temporal patches that capture local patterns. We project each patch through a learnable linear layer and add a learnable positional encoding along the time axis for each channel to generate tokens. Finally, we permute the data dimensions so that the patch sequence comes first, then flatten the tokens across the patch and channel dimensions to create a unified sequence. This enables the Transformer to model all pairwise dependencies (see Panel A, Figure 1). We apply this permutation to simplify the structure of the attention mask, making it easier to analyze further (see App. C.1).
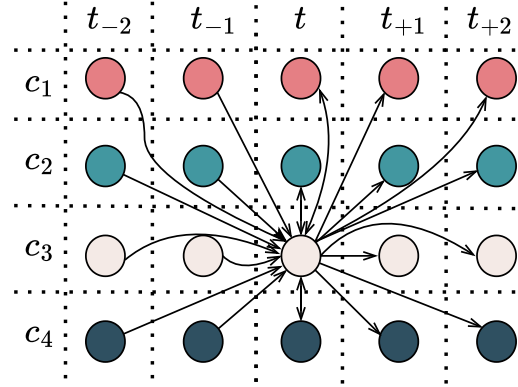
Figure 2: Potential cross-channel and temporal dependencies for token at channel 3 at time t.

4.2 Cross-Relational Attention Block (CRAB)

CRAB modifies the standard attention (Vaswani et al., 2017) block with two complementary components designed to increase models expressivity: (i) a learnable, non-Boolean relational mask designed to learn important dependencies, and (ii) a signed, absolute-sum normalization activation function that replaces the original softmax, designed to increase expressiveness by allowing negative values, inspired by Lv et al. (2024) findings. For a visual representation of the model refer to Panel B.1, Fig. 1.

Our **learnable non-Boolean mask** is designed to learn the most dominant dependencies between tokens. We apply this mask to a *positive-transformed* attention score matrix. Starting from the score matrix $A \in \mathbb{R}^{N \times N}$, we remove sign information via a global shift,

$$A_+ = A - \min(A) .$$

Then, we initialize a learnable real-valued mask $M \in \mathbb{R}^{N \times N}$ with zero mean and standard deviation $\sqrt{2/N}$ following He initialization (He et al., 2015). We apply M in an element-wise fashion:

$$A = M \circ A_+ .$$

Thus, this shift removes sign while preserving the *relative ranking* and pairwise differences of the original scores, while the learnable mask M sets their signs and reweighs magnitudes. The produced output is then passed to the activation function.

Our **modified attention activation function** replaces softmax with a row-wise normalization that yields *signed* attention weights. Allowing negative weights can increase the model's expressive power (Lv et al., 2024). To ensure stable training, our proposed activation must preserve the stability property that underlies softmax's success (Saratchandran et al., 2025): maintaining a bounded Frobenius norm of $\sqrt{N}$ for the produced activation matrix,

$$\left\| \text{Activation}(A) \right\|_F \leq \sqrt{N} .$$

For an attention-score matrix $A \in \mathbb{R}^{N \times N}$, we define our activation function as a normalization of values by the absolute sum of the corresponding row. The AbsAct function is defined as:

$$\text{AbsAct}(A_{ij}) = \frac{A_{ij} + \varepsilon}{\sum_{k=1}^{N} |A_{ik} + \varepsilon| + \delta}, \quad \forall i, j \in \{1, \ldots, N\} \tag{1}$$

where $\varepsilon = 1 \times 10^{-4}$ and $\delta = 1 \times 10^{-8}$ are numerical stabilizers. The parameter ε shifts each attention score before normalization, while δ adds a positive margin to ensure the denominator remains non-zero. Our activation function satisfies the bounded-norm constraint, ensuring stable training (see Appendix A.1 for a formal proof). Additionally, by allowing negative attention weights, the model can capture more diverse dependencies, thereby increasing its expressiveness.

4.3 Dependency Compression Plugin (DeCoP)

Since we model all cross-channel and cross-time dependencies (Figure 2) using the attention mechanism, memory and compute scale as $\mathcal{O}(N^2)$, where N is the total number of modeled relations. Applying such attention on datasets with many channels, often exceeds hardware capacity and can prevent models from running. To address this limitation, we introduce *DeCoP*, a plugin which compresses each row of the attention matrix $A \in \mathbb{R}^{N \times N}$ with a learnable transformation, yielding a compressed matrix $A_c \in \mathbb{R}^{N \times k}$ with $k \ll N$. This reduces the dominant cost from quadratic to linear in N for fixed k, improving scalability regardless of dataset size. For a visual plot of the model, we refer to Panel B.2, Fig. 1. DeCoP is defined as follows:

DeCoP introduces a learnable compression transform whose parameters are initialized with He initialization (He et al., 2015) and fine-tuned during training. Our compressor is a matrix, $C \in \mathbb{R}^{N \times k}$ such that $k \ll N$. Let $Q = XW_q$, $K = XW_k$ with $Q, K \in \mathbb{R}^{N \times D_m}$. We utilize C in the attention computation as follows:

$$A_c = \frac{Q\left(K^\top C\right)}{\sqrt{D_m}} \in \mathbb{R}^{N \times k} .$$

Due to the associative property of matrix multiplication, computing $Q(K^\top C)$ is equivalent to computing $(QK^\top)C$, enabling us to obtain a compressed version of the full token-to-token attention without materializing the quadratic $N \times N$ attention matrix. While vanilla attention incurs $O(N^2 D_m)$ cost for computing $QK^\top$, DeCoP's reordered computation achieves $O(ND_m k)$ complexity, scaling linearly in N when $k \ll N$ while

preserving essential attention relationships through the compressed representation. For a full complexity analysis, see Appendix A.2.

Finally, we also need to modify V calculations as the attention dimension is reduced to k. The modification is defined as follows:

$$W_v \in \mathbb{R}^{k \times N} \ , \qquad V = W_v X, \quad V \in \mathbb{R}^{k \times D_m} \ .$$

The new V represents the values corresponding to the compressed attention dependencies. The final output is calculated as follows:

$$W_c = \text{AbsAct}(A_c) \in \mathbb{R}^{N \times k} \ , \qquad O = W_c V \in \mathbb{R}^{N \times D_m} \ .$$

5 Experiments

We evaluate the proposed XCTFormer across three fundamental time-series tasks: long-term forecasting, imputation and anomaly detection. Our experiments utilize well-established benchmark datasets commonly employed in prior work to ensure fair comparison with existing approaches. Across all experiments, we apply DeCoP (Sec. 4.3) to datasets with more than 60 channels; datasets with 60 or fewer channels use the plain CRAB module without DeCoP (Sec. 4.2). For each task, we present the experimental setup and datasets and report comparative results against strong baselines. The following subsections detail our experiments for each time-series task. App. B provides formal task formulations, extended training and evaluation details, including hyperparameter search protocol and values.

5.1 Long-Term Forecasting

Time series forecasting aims to predict future values from historical observations. We evaluate our model on seven widely used multivariate datasets, comprising four ETT subsets (ETTm1, ETTm2, ETTh1, ETTh2), Weather, Electricity (ECL), and Traffic, following Autoformer (Wu et al., 2021). We adopt the TimesNet setup (Wu et al., 2023) with a lookback window of 96 time-steps and forecasting horizons $\{96, 192, 336, 720\}$. We compare against twelve widely recognized forecasting models: (i) Transformer based: Autoformer (Wu et al., 2021), FEDformer (Zhou et al., 2022), Crossformer (Zhang & Yan, 2023), PatchTST (Nie et al., 2023), iTransformer (Liu et al., 2024); (ii) Linear/MLP based: DLinear (Zeng et al., 2023), TiDE (Das et al., 2023), TimeMixer (Wang et al., 2024a), MTLinear (Nochumsohn et al., 2025); (iii) Hybrid Transformer and Linear: LeDDAM (Yu et al., 2024); (iv) TCN based: SCINet (Liu et al., 2022a), TimesNet (Wu et al., 2023).

Table 1: Average long-term forecasting results comparison. We compare extensive competitive models under different prediction lengths. The presented results are averaged accross these four prediction horizons $\{96, 192, 336, 720\}$. Red indicates best performance (lowest error), blue indicates second best.

Models	XCTFormer (Ours)		MTLinear[1] (AISTATS 2025)		Leddam (ICML 2024)		TimeMixer (ICLR 2024)		iTransformer (ICLR 2024)		PatchTST (ICLR 2023)		Crossformer (ICLR 2023)		TiDE (TMLR 2023)		TimesNet (ICLR 2023)		DLinear (AAAI 2023)		SCINet (NeurIPS 2022)		FEDformer (ICML 2022)		Autoformer (NeurIPS 2021)	
Metric	MSE	MAE	MSE	MAE	MSE	MAE	MSE	MAE	MSE	MAE	MSE	MAE	MSE	MAE	MSE	MAE	MSE	MAE	MSE	MAE	MSE	MAE	MSE	MAE	MSE	MAE
ETT(Avg)	**0.364**	**0.386**	0.373	**0.387**	**0.367**	**0.387**	**0.367**	0.389	0.384	0.404	0.397	0.406	0.685	0.578	0.482	0.470	0.391	0.404	0.446	0.447	0.689	0.597	0.421	0.433	0.465	0.459
Weather	**0.237**	**0.267**	**0.238**	0.276	0.242	**0.272**	0.240	**0.272**	0.258	0.278	0.265	0.285	0.264	0.320	0.270	0.320	0.259	0.286	0.265	0.315	0.292	0.363	0.309	0.360	0.338	0.382
ECL[P]	**0.166**	**0.263**	0.198	0.283	**0.168**	**0.263**	0.182	0.273	0.178	**0.270**	0.216	0.318	0.244	0.334	0.252	0.344	0.193	0.304	0.225	0.319	0.268	0.365	0.213	0.327	0.227	0.364
Traffic[P]	**0.435**	**0.287**	0.621	0.372	0.467	0.294	0.485	0.297	**0.428**	**0.282**	0.529	0.341	0.667	0.426	0.760	0.473	0.620	0.336	0.625	0.383	0.804	0.509	0.609	0.376	0.628	0.379
1st Count	**3**	**3**	0	0	0	1	0	0	1	1	0	0	0	0	0	0	0	0	0	0	0	0	0	0	0	0

[1] Reported MTLinear results reflect the per-dataset best of MTNLinear and MTDLinear (Nochumsohn et al., 2025).
[P] DeCoP was enabled for XCTFormer on this dataset.

Results. As shown in Table 1, XCTFormer delivers superior results to widely recognized baselines across diverse benchmarks, with best performance on 6 of 8 evaluation metrics. These gains highlight the model's effectiveness in capturing cross-channel dependencies in the long-term forecasting task.

Table 2: To evaluate our model performance on imputation, we randomly mask $\{12.5\%, 25\%, 37.5\%, 50\%\}$ of the time points in time series of length 1024. The final results are averaged across these 4 different masking ratios. Red indicates best performance (lowest error), blue indicates second best.

Models	XCTFormer (Ours)		TimeMixer++ (ICLR 2025)		TimeMixer (ICLR 2024)		iTransformer (ICLR 2024)		PatchTST (ICLR 2023)		Crossformer (ICLR 2023)		FEDformer (ICML 2022)		TIDE (TMLR 2023)		DLinear (AAAI 2023)		TimesNet (ICLR 2023)		MICN (ICLR 2023)		Autoformer (NeurIPS 2021)	
Metric	MSE	MAE	MSE	MAE	MSE	MAE	MSE	MAE	MSE	MAE	MSE	MAE	MSE	MAE	MSE	MAE	MSE	MAE	MSE	MAE	MSE	MAE	MSE	MAE
ETT(Avg)	**0.046**	**0.138**	0.055	0.154	0.097	0.220	0.096	0.205	0.120	0.225	0.150	0.258	0.124	0.230	0.314	0.366	0.115	0.229	0.079	0.182	0.119	0.234	0.104	0.215
Weather	**0.031**	**0.050**	0.049	0.078	0.091	0.114	0.095	0.102	0.082	0.149	0.150	0.111	0.064	0.139	0.063	0.131	0.071	0.107	0.061	0.098	0.075	0.126	0.066	0.107
ECL[p]	**0.046**	**0.141**	0.109	0.197	0.142	0.261	0.140	0.223	0.129	0.198	0.125	0.204	0.181	0.314	0.182	0.202	0.080	0.200	0.135	0.255	0.138	0.246	0.141	0.234

[p] DeCoP was enabled for XCTFormer on this dataset.

5.2 Imputation

Time-series imputation reconstructs missing values from observed data. We evaluate our model on six widely used multivariate datasets: four ETT subsets (ETTm1, ETTm2, ETTh1, ETTh2) (Zhou et al., 2021), Electricity (ECL), and Weather. We adopt the TimeMixer++ setup, using a lookback window of 1024 time-steps and applying random missing masks at rates $\{12.5\%, 25\%, 37.5\%, 50\%\}$. We compare against eleven widely recognized models: (i) Transformer-based: Autoformer (Wu et al., 2021), FEDformer (Zhou et al., 2022), Crossformer (Zhang & Yan, 2023), PatchTST (Nie et al., 2023), iTransformer (Liu et al., 2024); (ii) MLP-based: DLinear (Zeng et al., 2023), TiDE (Das et al., 2023), TimeMixer (Wang et al., 2024a); (iii) Convolutional-based: SCINet (Liu et al., 2022a), TimesNet (Wu et al., 2023), MICN (Wang et al., 2023).

Results. As shown in Table 2, XCTFormer delivers state-of-the-art (SoTA) results in comparison to competing baselines across diverse benchmarks. With the best performance on all 6 evaluation metrics. Particularly, our approach outperforms the second-best baseline by an average of 24.1% on MSE and 17.6% on MAE across all datasets, highlighting the model's effectiveness in capturing cross-channel dependencies.

5.3 Anomaly Detection

Anomaly detection seeks to identify unusual or abnormal patterns in time-series, often corresponding to faults, attacks, or rare operational modes. We evaluate on five widely used benchmarks: SMD (Server Machine Dataset, (Su et al., 2019)) , SWaT (Secure Water Treatment, (Mathur & Tippenhauer, 2016)), PSM (Pooled Server Metrics, (Abdulaal et al., 2021)), and NASA telemetry datasets MSL and SMAP (Hundman et al., 2018). We compare against nineteen widely used models: (i) RNN/TCN: LSTM (Hochreiter & Schmidhuber, 1997), TCN (Franceschi et al., 2019); (ii) Transformer-based: Transformer (Vaswani et al., 2017), LogTrans (Li et al., 2019a), Reformer (Kitaev et al., 2020), Informer (Zhou et al., 2021), Pyraformer (Liu et al., 2022b), Autoformer (Wu et al., 2021), FEDformer (Zhou et al., 2022), ETSformer (Woo et al., 2022), Stationary (Non-stationary Transformer) (Liu et al., 2022c), Anomaly Transformer (Xu et al., 2022), LightTS (Zhang et al., 2022), iTransformer (Liu et al., 2024); (iii) State-space: LSSL (Gu et al., 2022); (iv) Linear/MLP: DLinear (Zeng et al., 2023), TiDE (Das et al., 2023); (v) Convolutional/Mixer: TimesNet (Wu et al., 2023), TimeMixer++ (Wang et al., 2025).

Results. As shown in Table 3, XCTFormer performs competitively against the considered strong baselines. Our model attains the overall best F_1, demonstrating its superior ability to capture cross-channel dependencies in the anomaly detection task.

6 Analysis

Ablation Study. To evaluate the contribution of each component in XCTFormer, we conducted a comprehensive ablation study across three fundamental time-series tasks: long-term forecasting, imputation and anomaly detection. These tasks represent diverse aspects of time-series analysis, enabling comprehensive evaluation of our proposed components' necessity. Our methodology involved two categories of experiments: (i) *component-wise analysis*, where we systematically removed or altered individual architectural modifications

Table 3: Full results for the anomaly detection task. The P, R, and F1 represent the precision, recall, and F1-score, (%) respectively. F1-score is the harmonic mean of precision and recall. A higher value of P, R and F1 indicates a better performance. Red indicates highest F1 score, blue indicates second highest F1 score.

Datasets		SMD			MSL			SMAP			SWaT			PSM			Avg F1
Metrics		P	R	F1	P	R	F1	P	R	F1	P	R	F1	P	R	F1	(%)
LSTM	(1997)	78.52	65.47	71.41	78.04	86.22	81.93	91.06	57.49	70.48	78.06	91.72	84.34	69.24	99.53	81.67	77.97
Transformer	(2017)	83.58	76.13	79.56	71.57	87.37	78.68	89.37	57.12	69.70	68.84	96.53	80.37	62.75	96.56	76.07	76.88
LogTrans	(2019a)	83.46	70.13	76.21	73.05	87.37	79.57	89.15	57.59	69.97	68.67	97.32	80.52	63.06	98.00	76.74	76.60
TCN	(2019)	84.06	79.07	81.49	75.11	82.44	78.60	86.90	59.23	70.45	76.59	95.71	85.09	54.59	99.77	70.57	77.24
Reformer	(2020)	82.58	69.24	75.32	85.51	83.31	84.40	90.91	57.44	70.40	72.50	96.53	82.80	59.93	95.38	73.61	77.31
Informer	(2021)	86.60	77.23	81.65	81.77	86.48	84.06	90.11	57.13	69.92	70.29	96.75	81.43	64.27	96.33	77.10	78.83
Anomaly*	(2022)	88.91	82.23	85.49	79.61	87.37	83.31	91.85	58.11	71.18	72.51	97.32	83.10	68.35	94.72	79.40	80.50
Pyraformer	(2022b)	85.61	80.61	83.04	83.81	85.93	84.86	92.54	57.71	71.09	87.92	96.00	91.78	71.67	96.02	82.08	82.57
Autoformer	(2021)	88.06	82.35	85.11	77.27	80.92	79.05	90.40	58.62	71.12	89.85	95.81	92.74	99.08	88.15	93.29	84.26
LSSL	(2022)	78.51	65.32	71.31	77.55	88.18	82.53	89.43	53.43	66.90	79.05	93.72	85.76	66.02	92.93	77.20	76.74
Stationary	(2022c)	88.33	81.21	84.62	68.55	89.14	77.50	89.37	59.02	71.09	68.03	96.75	79.88	97.82	96.76	97.29	82.08
DLinear	(2023)	83.62	71.52	77.10	84.34	85.42	84.88	92.32	55.41	69.26	80.91	95.30	87.52	98.28	89.26	93.55	82.46
ETSformer	(2022)	87.44	79.23	83.13	85.13	84.93	85.03	92.25	55.75	69.50	90.02	80.36	84.91	99.31	85.28	91.76	82.87
LightTS	(2022)	87.10	78.42	82.53	82.40	75.78	78.95	92.58	55.27	69.21	91.98	94.72	93.33	98.37	95.97	97.15	84.23
FEDformer	(2022)	87.95	82.39	85.08	77.14	80.07	78.57	90.47	58.10	70.76	90.17	96.42	93.19	97.31	97.16	97.23	84.97
TimesNet	(2023)	88.66	83.14	85.81	83.92	86.42	85.15	92.52	58.29	71.52	86.76	97.32	91.74	98.19	96.76	97.47	86.34
TiDE	(2023)	76.00	63.00	68.91	84.00	60.00	70.18	88.00	50.00	64.00	98.00	63.00	76.73	93.00	92.00	92.50	74.46
iTransformer	(2024)	78.45	65.10	71.15	86.15	62.65	72.54	90.67	52.96	66.87	99.96	65.55	79.18	95.65	94.69	95.17	76.98
TimesMixer++	(2025)	88.59	84.50	86.50	89.73	82.23	85.82	93.47	60.02	73.10	92.96	94.33	94.64	98.33	96.90	97.60	87.47
XCTFormer	(Ours)	86.94	81.64	84.21	89.46	70.81	79.05	93.79	80.57	86.68	92.25	92.96	92.60	98.26	92.52	95.30	87.57

∗ The original paper of Anomaly Transformer (Xu et al., 2022) adopts the temporal association and reconstruction error as a joint anomaly criterion. For fair comparisons, we only use reconstruction error here.

introduced to the vanilla Transformer to isolate each component's impact. Modifications include: removing the learnable mask, reverting the activation function from our proposed approach back to the standard softmax and both; (ii) *dependency modeling analysis*, where we examined variants that model only cross-channel dependencies (inspired by iTransformer (Liu et al., 2024)) or only temporal relationships (similar to PatchTST (Nie et al., 2023)) to validate the necessity of our integrated cross-channel and cross-time modeling strategy. Results presented in Table 4 report the average performance metrics across all datasets and experimental configurations specific to each task for every model variation. The full XCTFormer consistently outperforms all variants across all three tasks and evaluation metrics. These findings validate our architectural design choices and provide empirical evidence that each proposed component contributes meaningfully to the model's overall performance across diverse time-series applications. For detailed experimental configurations and full results, refer to Appendix D.1.

Table 4: Ablation study results across different tasks, evaluated with different XCTFormer variations.

	Long-term Forecasting		Imputation		Anomaly Detection			XCTFormer vs Others
	MSE	MAE	MSE	MAE	Precision	Recall	F-Score	(%)
XCTFormer (Original)	**0.328**	**0.337**	**0.044**	**0.124**	**92.1**	**83.7**	**87.6**	-
W/o mask	0.338	0.344	0.050	0.132	90.6	74.5	81.1	6.7%
Original softmax activation	0.359	0.364	0.053	0.143	90.3	75.4	81.5	9.7%
Vanilla transformer	0.361	0.364	0.060	0.149	90.9	76.1	82.0	11.2%
Sequence modeling	0.341	0.343	0.052	0.131	91.2	78.8	83.9	5.6%
Channel modeling	0.341	0.348	0.081	0.174	91.2	76.1	82.3	14.2%

Robustness Across Random Seeds. To evaluate the stability and reliability of XCTFormer, we assessed its performance across different random initializations. Neural models are often sensitive to the randomness of parameter initialization and the order of training samples, which can cause variability in results. To address this, we trained XCTFormer using the optimal hyperparameters selected by validation on five distinct random seeds (2021 to 2025). For each of the three primary time series tasks: long-term forecasting, anomaly detection, and imputation, we report both the mean and standard deviation of the relevant performance metric, providing a more robust estimate of model effectiveness. We further quantify robustness using a confidence score calculated best on coefficient of variation (Reed et al., 2002), which expresses the model's precision and repeatability. In this context, a lower standard deviation signifies greater consistency and therefore higher reliability. Summarized seed robustness results are presented in Table 5. For more information on confidence score calculation and the complete analysis tables, refer to Appendix D.2.

Table 5: Averaged metrics of trained models, evaluated on five different seeds (2021–2025) across all datasets, are reported for each metric and time-series task, along with the corresponding confidence interval.

Task	Metric	Mean $\pm$ Avg. Std	Confidence Score (%)
Long-Term Forecasting	MSE	0.3304 ± 0.0031	99.05%
Long-Term Forecasting	MAE	0.3387 ± 0.0024	99.28%
Imputation	MSE	0.04683 ± 0.00509	89.14%
Imputation	MAE	0.1280 ± 0.00883	93.10%
Anomaly Detection	Precision	91.382 ± 0.868	99.05%
Anomaly Detection	Recall	79.660 ± 4.298	94.60%
Anomaly Detection	F1	84.600 ± 3.100	96.34%

7 Conclusion

In this paper, we address a fundamental paradox in multivariate time-series analysis: while cross-channel dependencies should theoretically improve model performance by leveraging cross-channel dependencies, recent findings reveal that channel-independent (CI) models often outperform channel-dependent (CD) models. This counterintuitive result suggests that existing CD methods fail to realize the full potential of cross-channel information. We argue that this limitation stems from current approaches modeling cross-channel and cross-time dependencies *indirectly*, leading to potential information loss and overlooked critical interactions. To bridge this gap, we introduce **XCTFormer**, which revisits channel dependence by adopting a direct, token-by-token modeling approach. Specifically, instead of treating channels and time-steps as separate entities processed through multi-stage pipelines, our approach represents each data point (channel-time combination) as an individual token and models all pairwise dependencies between these tokens simultaneously within a unified attention mechanism. This is particularly important for capturing evolving dependencies between channels throughout time. Through the Cross-Relational Attention Block (CRAB) with learnable masking and enhanced attention activation function, XCTFormer achieves improved expressivity while maintaining robustness, with the optional Dependency Compression Plugin (DeCoP) enabling scalability for high-dimensional datasets. Extensive evaluation across forecasting, anomaly detection, and imputation tasks demonstrates XCTFormer's effectiveness, achieving average error reductions of 24.1% in MSE and 17.6% in MAE for imputation alongside notable improvements in forecasting and anomaly detection. This direct modeling approach marks a significant step toward comprehensively capturing dependencies and realizing the full theoretical potential of multivariate time-series modeling.

References

Ahmed Abdulaal, Zhuanghua Liu, and Tomer Lancewicki. Practical Approach to Asynchronous Multivariate Time Series Anomaly Detection and Localization. In *Proceedings of the 27th ACM SIGKDD Conference on Knowledge Discovery and Data Mining*, 2021.

George E. P. Box and Gwilym M. Jenkins. *Time Series Analysis: Forecasting and Control*. Holden-Day, first edition, 1970.

Gilbert Brunet, David B Parsons, Dimitar Ivanov, Boram Lee, Peter Bauer, Natacha B Bernier, Veronique Bouchet, Andy Brown, Antonio Busalacchi, Georgina Campbell Flatter, et al. Advancing weather and climate forecasting for our changing world. *Bulletin of the American Meteorological Society*, 2023.

C Bui, N Pham, A Vo, A Tran, A Nguyen, and T Le. Time series forecasting for healthcare diagnosis and prognostics with the focus on cardiovascular diseases. In *6th International Conference on the Development of Biomedical Engineering in Vietnam (BME6)*. Springer, 2018.

Xiaodan Chen, Xiucheng Li, Xinyang Chen, and Zhijun Li. Structured Matrix Basis for Multivariate Time Series Forecasting with Interpretable Dynamics. In *Annual Conference on Neural Information Processing Systems, NeurIPS*, 2024.

Abhimanyu Das, Weihao Kong, Andrew Leach, Shaan Mathur, Rajat Sen, and Rose Yu. Long-term Forecasting with TiDE: Time-series Dense Encoder. *Transactions on Machine Learning Research*, 2023.

Pedro Domingos. A Few Useful Things to Know about Machine Learning. *Communications of the ACM*, 2012.

Diego Duarte, Chris Walshaw, and Nadarajah Ramesh. A comparison of time-series predictions for healthcare emergency department indicators and the impact of COVID-19. *Applied Sciences*, 2021.

Jean-Yves Franceschi, Aymeric Dieuleveut, and Martin Jaggi. Unsupervised Scalable Representation Learning for Multivariate Time Series. In *Annual Conference on Neural Information Processing Systems, NeurIPS*, 2019.

Albert Gu, Karan Goel, and Christopher Ré. Efficiently Modeling Long Sequences with Structured State Spaces. In *International Conference on Learning Representations (ICLR)*, 2022.

Lu Han, Han-Jia Ye, and De-Chuan Zhan. The Capacity and Robustness Trade-Off: Revisiting the Channel Independent Strategy for Multivariate Time Series Forecasting. *IEEE Trans. Knowl. Data Eng.*, 36(11), 2024.

Kaiming He, Xiangyu Zhang, Shaoqing Ren, and Jian Sun. Delving Deep into Rectifiers: Surpassing Human-Level Performance on ImageNet Classification. In *IEEE International Conference on Computer Vision, ICCV*, 2015.

Sepp Hochreiter and Jürgen Schmidhuber. Long short-term memory. *Neural computation*, 1997.

Kyle Hundman, Valentino Constantinou, Christopher Laporte, Ian Colwell, and Tom Söderström. Detecting spacecraft anomalies using lstms and nonparametric dynamic thresholding. In *Proceedings of the 24th ACM SIGKDD International Conference on Knowledge Discovery and Data Mining*, 2018. Datasets: SMAP and MSL.

Berivan Isik, Natalia Ponomareva, Hussein Hazimeh, Dimitris Paparas, Sergei Vassilvitskii, and Sanmi Koyejo. Scaling Laws for Downstream Task Performance in Machine Translation. In *The Thirteenth International Conference on Learning Representations, ICLR*, 2025.

Ming Jin, Huan Yee Koh, Qingsong Wen, Daniele Zambon, Cesare Alippi, Geoffrey I. Webb, Irwin King, and Shirui Pan. A Survey on Graph Neural Networks for Time Series: Forecasting, Classification, Imputation, and Anomaly Detection. *IEEE TPAMI*, 2024.

Taesung Kim, Jinhee Kim, Yunwon Tae, Cheonbok Park, Jang-Ho Choi, and Jaegul Choo. Reversible Instance Normalization for Accurate Time-Series Forecasting against Distribution Shift. In *The Tenth International Conference on Learning Representations, ICLR*, 2022.

Diederik P. Kingma and Jimmy Ba. Adam: A Method for Stochastic Optimization. In *3rd International Conference on Learning Representations, ICLR*, 2015.

Nikita Kitaev, Łukasz Kaiser, and Anselm Levskaya. Reformer: The Efficient Transformer. In *International Conference on Learning Representations (ICLR)*, 2020.

Shiyang Li, Xiaoyong Jin, Yao Xuan, Xiyou Zhou, Wenhu Chen, Yu-Xiang Wang, and Xifeng Yan. Enhancing the Locality and Breaking the Memory Bottleneck of Transformer on Time Series Forecasting. In *Advances in Neural Information Processing Systems (NeurIPS)*, 2019a.

Shiyang Li, Xiaoyong Jin, Yao Xuan, Xiyou Zhou, Wenhu Chen, Yu-Xiang Wang, and Xifeng Yan. Enhancing the Locality and Breaking the Memory Bottleneck of Transformer on Time Series Forecasting. In *Annual Conference on Neural Information Processing Systems, NeurIPS*, 2019b.

Minhao Liu, Ailing Zeng, Muxi Chen, Zhijian Xu, Qiuxia Lai, Lingna Ma, and Qiang Xu. SCINet: Time Series Modeling and Forecasting with Sample Convolution and Interaction. In *Annual Conference on Neural Information Processing Systems, NeurIPS*, 2022a.

Shizhan Liu, Hang Yu, Cong Liao, Jianguo Li, Weiyao Lin, Alex X. Liu, and Schahram Dustdar. Pyraformer: Low-Complexity Pyramidal Attention for Long-Range Time Series Modeling and Forecasting. In *The Tenth International Conference on Learning Representations, ICLR*, 2022b.

Yong Liu, Haixu Wu, Jianmin Wang, and Mingsheng Long. Non-stationary transformers: Exploring the stationarity in time series forecasting. In *Advances in Neural Information Processing Systems (NeurIPS)*, 2022c.

Yong Liu, Tengge Hu, Haoran Zhang, Haixu Wu, Shiyu Wang, Lintao Ma, and Mingsheng Long. iTransformer: Inverted transformers are effective for time series forecasting. In *The Twelfth International Conference on Learning Representations, ICLR*, 2024.

Ang Lv, Ruobing Xie, Shuaipeng Li, Jiayi Liao, Xingwu Sun, Zhanhui Kang, Di Wang, and Rui Yan. More Expressive Attention with Negative Weights. *arXiv preprint arXiv:2411.07176*, 2024.

Aditya P. Mathur and Nils Ole Tippenhauer. SWaT: A Water Treatment Testbed for Research and Training on ICS Security. In *Proceedings of the International Workshop on Cyber-Physical Systems for Smart Water Networks*. IEEE, 2016.

Aristeidis Mystakidis, Paraskevas Koukaras, Nikolaos Tsalikidis, Dimosthenis Ioannidis, and Christos Tjortjis. Energy Forecasting: A Comprehensive Review of Techniques and Technologies. *Energies*, 2024.

Yuqi Nie, Nam H. Nguyen, Phanwadee Sinthong, and Jayant Kalagnanam. A Time Series is Worth 64 Words: Long-term Forecasting with Transformers. In *The Eleventh International Conference on Learning Representations, ICLR*, 2023.

Liran Nochumsohn, Hedi Zisling, and Omri Azencot. A Multi-Task Learning Approach to Linear Multivariate Forecasting. In *International Conference on Artificial Intelligence and Statistics, AISTATS*, 2025.

Adam Paszke, Sam Gross, Francisco Massa, Adam Lerer, James Bradbury, Gregory Chanan, Trevor Killeen, Zeming Lin, Natalia Gimelshein, Luca Antiga, Alban Desmaison, Andreas Köpf, Edward Z. Yang, Zachary DeVito, Martin Raison, Alykhan Tejani, Sasank Chilamkurthy, Benoit Steiner, Lu Fang, Junjie Bai, and Soumith Chintala. PyTorch: An Imperative Style, High-Performance Deep Learning Library. In *Annual Conference on Neural Information Processing Systems, NeurIPS*, 2019.

Gerald F. Reed, Frances Lynn, and Brian D. Meade. Use of the coefficient of variation in assessing variability in quantitative assays. *Clinical and Diagnostic Laboratory Immunology*, 2002.

Hemanth Saratchandran, Jianqiao Zheng, Yiping Ji, Wenbo Zhang, and Simon Lucey. Rethinking Attention: Polynomial Alternatives to Softmax in Transformers, 2025.

Ya Su, Youjian Zhao, Chenhao Niu, Rong Liu, Wei Sun, and Dan Pei. Robust Anomaly Detection for Multivariate Time Series through Stochastic Recurrent Neural Network. In *Proceedings of the 25th ACM SIGKDD International Conference on Knowledge Discovery and Data Mining*, 2019.

Patara Trirat, Yooju Shin, Junhyeok Kang, Youngeun Nam, Jihye Na, Minyoung Bae, Joeun Kim, Byunghyun Kim, and Jae-Gil Lee. Universal Time-Series Representation Learning: A Survey. *arXiv*, 2024.

Ashish Vaswani, Noam Shazeer, Niki Parmar, Jakob Uszkoreit, Llion Jones, Aidan N. Gomez, Lukasz Kaiser, and Illia Polosukhin. Attention is all you need. In *Annual Conference on Neural Information Processing Systems, NeurIPS*, 2017.

Huiqiang Wang, Jian Peng, Feihu Huang, Jince Wang, Junhui Chen, and Yifei Xiao. MICN: Multi-scale Local and Global Context Modeling for Long-term Series Forecasting. In *The Eleventh International Conference on Learning Representations, ICLR*, 2023.

Shiyu Wang, Haixu Wu, Xiaoming Shi, Tengge Hu, Huakun Luo, Lintao Ma, James Y. Zhang, and Jun Zhou. TimeMixer: Decomposable Multiscale Mixing for Time Series Forecasting. In *The Twelfth International Conference on Learning Representations, ICLR*, 2024a.

Shiyu Wang, Jiawei Li, Xiaoming Shi, Zhou Ye, Baichuan Mo, Wenze Lin, Shengtong Ju, Zhixuan Chu, and Ming Jin. TimeMixer++: A General Time Series Pattern Machine for Universal Predictive Analysis. In *The Thirteenth International Conference on Learning Representations, ICLR*, 2025.

Xinlin Wang, Hao Wang, Binayak Bhandari, and Leming Cheng. AI-Empowered Methods for Smart Energy Consumption: A Review of Load Forecasting, Anomaly Detection and Demand Response. *International Journal of Precision Engineering and Manufacturing-Green Technology*, 2024b.

Xue Wang, Tian Zhou, Qingsong Wen, Jinyang Gao, Bolin Ding, and Rong Jin. CARD: Channel Aligned Robust Blend Transformer for Time Series Forecasting. In *The Twelfth International Conference on Learning Representations, ICLR*, 2024c.

Gerald Woo, Chenghao Liu, Doyen Sahoo, Akshat Kumar, and Steven Hoi. ETSformer: Exponential Smoothing Transformers for Time-series Forecasting. *arXiv preprint arXiv:2202.01381*, 2022.

Haixu Wu, Jiehui Xu, Jianmin Wang, and Mingsheng Long. Autoformer: Decomposition transformers with auto-correlation for long-term series forecasting. In *Annual Conference on Neural Information Processing Systems 2021, NeurIPS*, 2021.

Haixu Wu, Tengge Hu, Yong Liu, Hang Zhou, Jianmin Wang, and Mingsheng Long. TimesNet: Temporal 2D-Variation Modeling for General Time Series Analysis. In *The Eleventh International Conference on Learning Representations, ICLR*, 2023.

Jiehui Xu, Haixu Wu, Jianmin Wang, and Mingsheng Long. Anomaly Transformer: Time Series Anomaly Detection with Association Discrepancy. In *International Conference on Learning Representations (ICLR)*, 2022.

Guoqi Yu, Jing Zou, Xiaowei Hu, Angelica I. Avilés-Rivero, Jing Qin, and Shujun Wang. Revitalizing Multivariate Time Series Forecasting: Learnable Decomposition with Inter-Series Dependencies and Intra-Series Variations Modeling. In *Forty-first International Conference on Machine Learning, ICML*, 2024.

Ailing Zeng, Muxi Chen, Lei Zhang, and Qiang Xu. Are transformers effective for time series forecasting? In *Thirty-Seventh Conference on Artificial Intelligence*. AAAI, 2023.

Tianping Zhang, Yizhuo Zhang, Wei Cao, Jiang Bian, Xiaohan Yi, Shun Zheng, and Jian Li. Less Is More: Fast Multivariate Time Series Forecasting with Light Sampling-oriented MLP Structures. *arXiv preprint arXiv:2207.01186*, 2022.

Yunhao Zhang and Junchi Yan. Crossformer: Transformer Utilizing Cross-Dimension Dependency for Multivariate Time Series Forecasting. In *The Eleventh International Conference on Learning Representations, ICLR*, 2023.

Lifan Zhao and Yanyan Shen. Rethinking Channel Dependence for Multivariate Time Series Forecasting: Learning from Leading Indicators. In *The Twelfth International Conference on Learning Representations, ICLR*, 2024.

Haoyi Zhou, Shanghang Zhang, Jieqi Peng, Shuai Zhang, Jianxin Li, Hui Xiong, and Wancai Zhang. Informer: Beyond Efficient Transformer for Long Sequence Time-Series Forecasting. In *Thirty-Fifth Conference on Artificial Intelligence.* AAAI, 2021.

Tian Zhou, Ziqing Ma, Qingsong Wen, Xue Wang, Liang Sun, and Rong Jin. FEDformer: Frequency Enhanced Decomposed Transformer for Long-term Series Forecasting. In *International Conference on Machine Learning, ICML*, 2022.

A Appendix: Extended Notes on XCTFormer

A.1 Theoretical validity of the proposed activation function

Proof. We show that the proposed AbsAct activation function satisfies the sufficient stability criterion of Saratchandran et al. (2025), namely that the Frobenius norm of the produced matrix is bounded by the square root of the number of rows:

$$\|\mathbf{Activation}(A)\|_F \leq \sqrt{N}$$

Given a matrix $A = (a_{ij}) \in \mathbb{R}^{N \times N}$, and using the activation defined in Section 4, we have:

$$\mathbf{AbsAct}\left(\begin{bmatrix} a_{11} & \cdots & a_{1n} \\ \vdots & \ddots & \vdots \\ a_{n1} & \cdots & a_{nn} \end{bmatrix}\right) = \begin{bmatrix} \dfrac{a_{11}}{\sum_{j=1}^{n}|a_{1j}|} & \cdots & \dfrac{a_{1n}}{\sum_{j=1}^{n}|a_{1j}|} \\ \vdots & \ddots & \vdots \\ \dfrac{a_{n1}}{\sum_{j=1}^{n}|a_{nj}|} & \cdots & \dfrac{a_{nn}}{\sum_{j=1}^{n}|a_{nj}|} \end{bmatrix}. \tag{2}$$

Note. In practice, we add a small positive offset and a denominator stabilizer to prevent division by zero. We set $\tilde{a}_{ij} = a_{ij} + 10^{-4}$ element-wise, then normalize each row by $\sum_{j=1}^{n}|\tilde{a}_{ij}| + 10^{-8}$, i.e., use $\tilde{a}_{ij} / \left(\sum_{k=1}^{n}|\tilde{a}_{ik}| + 10^{-8}\right)$. These constants ($10^{-4}$ and 10^{-8}) are included only for numerical stability and are omitted from the proof for simplicity.

By definition of the Frobenius Norm:

$$\|\mathbf{AbsAct}(A)\|_F^2 = \sum_{i=1}^{N}\sum_{j=1}^{n}\left(\frac{a_{ij}}{\sum_{k=1}^{n}|a_{ik}|}\right)^2 \tag{3}$$

$$= \sum_{i=1}^{N} \frac{\sum_{j=1}^{n} a_{ij}^2}{\left(\sum_{k=1}^{n}|a_{ik}|\right)^2} \tag{4}$$

$$\leq \sum_{i=1}^{N} \frac{\left(\sum_{j=1}^{n}|a_{ij}|\right)^2}{\left(\sum_{k=1}^{n}|a_{ik}|\right)^2} \quad \left(\text{since } \sum_j x_j^2 \leq \left(\sum_j |x_j|\right)^2\right) \tag{5}$$

$$= \sum_{i=1}^{N} 1 \; = \; N. \tag{6}$$

Hence, $\|\mathbf{AbsAct}(A)\|_F \leq \sqrt{N}$.
Note. The same bound holds when DeCoP is applied: the matrix still has N rows, and after rowwise ℓ_1 normalization each row's Frobenius norm is strictly less than one. Consequently, the sum of the Frobenius norm across all rows, does not exceed N.

$\square$

A.2 DeCoP: Complexity Analysis

We show that DeCoP reduces the attention cost from *quadratic* in the sequence length N to *linear* (for fixed $k \ll N$), lowering both compute and memory.

Setup. Let $X \in \mathbb{R}^{N \times D_i}$ and $W_q, W_k \in \mathbb{R}^{D_i \times D_m}$. Define

$$Q = XW_q \in \mathbb{R}^{N \times D_m}, \qquad K = XW_k \in \mathbb{R}^{N \times D_m}.$$

DeCoP introduces a learnable compression matrix $C \in \mathbb{R}^{N \times k}$ with $k \ll N$.

DeCoP computation (no $N \times N$ intermediate).

$$S = K^\top C \in \mathbb{R}^{D_m \times k}, \qquad A = \frac{QS}{\sqrt{D_m}} \in \mathbb{R}^{N \times k}.$$

CRAB Operations Starting from the score matrix $A \in \mathbb{R}^{N \times N}$, we remove sign information via a global shift,

$$A_+ = A - \min(A).$$

Then, the learnable non-boolean mask is applied element-wise:

$$A = M \circ A_+.$$

This contributes $O(Nk)$ compute and $O(Nk)$ parameters.

Total complexity.

$$
\begin{aligned}
\text{Total} = {} & O(ND_iD_m) && \text{(form } Q) \\
& + O(ND_iD_m) && \text{(form } K) \\
& + O(ND_mk) && (S = K^\top C) \\
& + O(ND_mk) && (A = QS/\sqrt{D_m}) \\
& + O(Nk) && \text{(global shift to } A_+) \\
& + O(Nk) && \text{(element-wise gate } M \circ A_+) \\
= {} & O\big(N[\,2D_iD_m + 2D_mk + 2k\,]\big) = O\big(2ND_iD_m + 2ND_mk\big) && \text{(dropping lower-order } Nk) \\
\overset{(D_i=D_m)}{=} {} & \boxed{O\big(N(D_m^2 + D_mk)\big)}.
\end{aligned}
$$

Growth in N. For fixed D_i, D_m, k with $k \ll N$, the cost is linear in N.

Memory. Store Q, K: $O(ND_m)$; A and A_+: $O(Nk)$; temporary S: $O(D_mk)$; parameters C: $O(Nk)$, M: $O(Nk)$. No $N \times N$ matrix is materialized.

B   Appendix: Implementation Details

B.1   Time-Series Tasks Formulation and Metrics

This section presents the mathematical formulation and evaluation metrics for three fundamental time-series tasks: long-term forecasting, anomaly detection, and imputation. Each task addresses distinct challenges in temporal data analysis while sharing common architectural foundations.

B.1.1   Long-Term Forecasting

Long-term forecasting aims to predict future values of a multivariate time series given historical observations. Given a historical sequence $\mathbf{X} \in \mathbb{R}^{L \times C}$ where L is the lookback window length and C is the number of channels, the objective is to predict the future sequence $\mathbf{Y} \in \mathbb{R}^{H \times C}$ where H is the prediction horizon.

Training Objective: The model minimizes the Mean Squared Error (MSE) loss:

$$\mathcal{L}_{forecast} = \frac{1}{N} \sum_{i=1}^{N} ||\mathbf{Y}_i - \hat{\mathbf{Y}}_i||^2 \tag{7}$$

where N is the number of training samples, $\mathbf{Y}_i$ is the ground truth, and $\hat{\mathbf{Y}}_i$ is the predicted sequence.

Evaluation Metrics: Performance is assessed using multiple regression metrics:

- **Mean Absolute Error (MAE):** $MAE = \frac{1}{NH} \sum_{i=1}^{N} \sum_{t=1}^{H} |\mathbf{Y}_{i,t} - \hat{\mathbf{Y}}_{i,t}|$
- **Mean Squared Error (MSE):** $MSE = \frac{1}{NH} \sum_{i=1}^{N} \sum_{t=1}^{H} (\mathbf{Y}_{i,t} - \hat{\mathbf{Y}}_{i,t})^2$

B.1.2   Imputation

Time-series imputation reconstructs missing values in partially observed sequences. Let $\mathbf{X} \in \mathbb{R}^{L \times C}$ be the ground-truth sequence and $\mathbf{M} \in \{0,1\}^{L \times C}$ a binary mask where $M_{t,c} = 0$ marks a missing entry; the observed input is obtained via an element-wise product $\mathbf{X}^{\text{obs}} = \mathbf{X} \odot \mathbf{M}$.

Problem Formulation. An imputation model with parameters ψ reconstructs the complete sequence:

$$\widehat{\mathbf{X}} = \text{Imputer}_{\psi}\big(\mathbf{X}^{\text{obs}}, \mathbf{M}\big) . \tag{8}$$

Training Objective. During training, artificial masks are sampled with mask rate p. The reconstruction loss is computed *only on masked positions*:

$$\mathcal{L}_{\text{impute}} = \frac{1}{|m|} \sum_{(t,c) \in m} \big(\mathbf{X}_{t,c} - \widehat{\mathbf{X}}_{t,c}\big)^2, \qquad m = \{(t,c) : M_{t,c} = 0\}. \tag{9}$$

Evaluation Protocol.

1. Apply a random mask (rate p) to test sequences to obtain $\mathbf{X}^{\text{obs}}$ and $\mathbf{M}$.
2. Impute the missing entries: $\mathbf{X}^{\text{filled}} = \mathbf{X}^{\text{obs}} \odot \mathbf{M} + \widehat{\mathbf{X}} \odot (1 - \mathbf{M})$.
3. Compute metrics *exclusively on the masked set m*.

Evaluation Metrics (masked-only). All metrics are calculated *only on masked values* $(t,c) \in m$:

$$\text{MAE}_{\text{mask}} = \frac{1}{|m|} \sum_{(t,c) \in m} \big|\mathbf{X}_{t,c} - \widehat{\mathbf{X}}_{t,c}\big|, \tag{10}$$

$$\text{MSE}_{\text{mask}} = \frac{1}{|m|} \sum_{(t,c) \in m} \big(\mathbf{X}_{t,c} - \widehat{\mathbf{X}}_{t,c}\big)^2. \tag{11}$$

B.1.3 Anomaly Detection

Anomaly detection identifies unusual patterns or outliers in time-series data using a reconstruction-based approach. The model learns to reconstruct normal patterns and flags samples with high reconstruction errors as anomalous.

Problem Formulation: Given a time series $\mathbf{X} \in \mathbb{R}^{L \times C}$, the model g_ϕ learns to reconstruct the input:

$$\hat{\mathbf{X}} = g_\phi(\mathbf{X}) \tag{12}$$

The anomaly score is computed as the reconstruction error: $s = ||\mathbf{X} - \hat{\mathbf{X}}||^2$

Training Objective: The model is trained exclusively on normal data using reconstruction loss:

$$\mathcal{L}_{recon} = \frac{1}{N} \sum_{i=1}^{N} ||\mathbf{X}_i - g_\phi(\mathbf{X}_i)||^2 \tag{13}$$

Detection Mechanism: We use a percentile-based threshold over the pooled anomaly-score distribution. Let $\mathcal{S} = \{s_{\text{train}}\} \cup \{s_{\text{test}}\}$. For a target anomaly rate α, the threshold is

$$\tau = \text{quantile}(\mathcal{S}, 1 - \alpha).$$

In our experiments we set $\alpha = 0.01$ (1%) for all datasets, except SMD (Su et al., 2019), where $\alpha = 0.005$ (0.5%). A sample with score s is labeled as

$$\text{label} = \begin{cases} 1, & \text{if } s > \tau \text{ (anomaly)}, \\ 0, & \text{if } s \leq \tau \text{ (normal)}. \end{cases}$$

Evaluation Metrics: Performance is measured using binary classification metrics:

- **Precision:** $P = \frac{TP}{TP+FP}$ (proportion of correctly identified anomalies)

- **Recall:** $R = \frac{TP}{TP+FN}$ (proportion of actual anomalies detected)

- **F1-Score:** $F_1 = 2 \cdot \frac{P \times R}{P+R}$ (harmonic mean of precision and recall)

- **Accuracy:** $Acc = \frac{TP+TN}{TP+TN+FP+FN}$ (overall classification correctness)

where TP, TN, FP, and FN represent true positives, true negatives, false positives, and false negatives, respectively.

B.2 Experiment Datasets And Evaluation Setups

We evaluate long-term forecasting on seven widely used multivariate datasets (Weather, Electricity, Traffic, ETTh1, ETTh2, ETTm1, ETTm2). For forecasting, we follow the TimesNet (Wu et al., 2023) setup with a look-back window $L = 96$ and horizons $H \in \{96, 192, 336, 720\}$; dataset specifications appear in Table 6. For time-series imputation, we use the same datasets as forecasting except Traffic and follow the TimeMixer++ (Wang et al., 2025) setup with $L = 1024$ and masking ratios $p \in \{12.5\%, 25\%, 37.5\%, 50\%\}$, for more detail refer to Table 7. Anomaly detection focuses on identifying fine-grained patterns. To assess this, we selected the following datasets: SMD (Server Machine Dataset, (Su et al., 2019)), SWaT (Secure Water Treatment, (Mathur & Tippenhauer, 2016)), PSM (Pooled Server Metrics, (Abdulaal et al., 2021)), and NASA telemetry datasets MSL and SMAP (Hundman et al., 2018). The details of the datasets used for anomaly detection are provided in Table 8. The details of the datasets used for anomaly detection are provided in Table 8.

Table 6: Benchmark datasets and evaluation settings for long-term forecasting.

Dataset	Dim	Look-back	Prediction Horizons	Dataset Size	Frequency	Information
ETTm1	7	96	{96, 192, 336, 720}	(34465, 11521, 11521)	15 min	Temperature
ETTm2	7	96	{96, 192, 336, 720}	(34465, 11521, 11521)	15 min	Temperature
ETTh1	7	96	{96, 192, 336, 720}	(8545, 2881, 2881)	15 min	Temperature
ETTh2	7	96	{96, 192, 336, 720}	(8545, 2881, 2881)	15 min	Temperature
Weather	21	96	{96, 192, 336, 720}	(36792, 5271, 10540)	10 min	Weather
Electricity	321	96	{96, 192, 336, 720}	(18317, 2633, 5261)	Hourly	Electricity
Traffic	862	96	{96, 192, 336, 720}	(12185, 1757, 3509)	Hourly	Transportation

Table 7: Benchmark datasets and evaluation settings for time-series imputation.

Dataset	Dim	Look-back	Imputation Mask Ratios	Dataset Size	Frequency	Information
ETTm1	7	1024	[12.5%, 25%, 37.5%, 50%]	(34465, 11521, 11521)	15 min	Temperature
ETTm2	7	1024	[12.5%, 25%, 37.5%, 50%]	(34465, 11521, 11521)	15 min	Temperature
ETTh1	7	1024	[12.5%, 25%, 37.5%, 50%]	(8545, 2881, 2881)	15 min	Temperature
ETTh2	7	1024	[12.5%, 25%, 37.5%, 50%]	(8545, 2881, 2881)	15 min	Temperature
Weather	21	1024	[12.5%, 25%, 37.5%, 50%]	(36792, 5271, 10540)	10 min	Weather
Electricity	321	1024	[12.5%, 25%, 37.5%, 50%]	(18317, 2633, 5261)	Hourly	Electricity

Table 8: Dataset detailed descriptions for anomaly detection. The dataset size is organized in (Train, Validation, Test).

Dataset	Dim	Series Length	Dataset Size	Information
SMD	38	100	(566724, 141681, 708420)	Server machines
MSL	55	100	(44653, 11664, 73729)	Spacecraft telemetry (Mars)
SMAP	25	100	(108146, 27037, 427617)	Spacecraft telemetry
SWaT	51	100	(396000, 99000, 449919)	Water treatment ICS
PSM	25	100	(105984, 26497, 87841)	Server metrics

B.3 Training Details.

All experiments were implemented in PyTorch (Paszke et al., 2019) and run on NVIDIA RTX 3090 GPUs. We fix the random seed to 2021. We applied a RevIN transformation (Kim et al., 2022) to mitigate distributional shifts in the data. Models are trained with the Adam optimizer (Kingma & Ba, 2015) using mean squared error (MSE) loss, together with a `OneCycleLR` scheduler. At a high level, `OneCycleLR` first increases the learning rate from its initial value to a peak (while inversely adjusting momentum), and then gradually anneals it to a small value for the remainder of training; this promotes fast early progress and stable late-stage convergence. We set `pct_start` = 0.4, allocating 40% of the total training steps to the warm-up/increase phase and 60% to the annealing phase. For each run, we select the checkpoint with the lowest validation MSE and report the corresponding test performance in the tables. We tuned hyperparameters with Optuna and retained the configuration yielding the lowest validation MSE; the resulting configuration is shared across all forecasting horizons (forecasting) or mask ratios (imputation) for each dataset and task, as presented in Table 9. For baselines evaluated under identical experimental settings to our main study, we report the results as published in the papers.

Table 9: Hyperparameter settings for **XCTFormer** per dataset per time-series task

| Dataset | Data Processing | | Transformer | | | | | | XCTFormer | | Training | | |
	patch_len	stride	e_layers	n_heads	d_model	d_ff	dropout	fc_dropout	attn_dropout	k	batch_size	learning_rate	epochs
Long-term Time Series Forecasting													
ETTh1	16	8	1	1	8	16	0.2	0.3	0.6	-	32	0.001	10
ETTh2	16	8	3	1	30	60	0.1	0.2	0.8	-	32	0.01	10
ETTm1	16	8	2	4	32	64	0.1	0.05	0.8	-	32	0.005	10
ETTm2	16	8	1	1	224	448	0.1	0.05	0.8	-	32	0.005	10
Weather	16	8	3	2	248	496	0.1	0.05	0.8	-	32	0.0005	10
Traffic	16	8	3	4	248	496	0.1	0.05	0.6	192	8	0.001	10
Electricity	16	8	3	1	248	496	0.1	0.05	0.5	64	32	0.005	10
Imputation													
ETTh1	16	8	2	1	64	128	0.1	0.05	0.5	-	32	0.01	10
ETTh2	64	32	3	1	160	320	0.1	0.05	0.3	-	32	0.005	10
ETTm1	16	8	3	4	96	192	0.1	0.05	0.1	-	32	0.005	10
ETTm2	16	8	2	1	128	256	0.1	0.05	0.5	-	32	0.001	10
Weather	16	8	3	1	192	384	0.1	0.05	0.8	-	32	0.001	10
Electricity	64	32	2	2	192	384	0.1	0.05	0.7	128	32	0.005	10
Anomaly Detection													
MSL	16	8	2	4	256	512	0.1	0.05	0.7	-	128	0.01	10
PSM	16	8	2	1	256	512	0.1	0.05	0.8	-	128	0.001	10
SMAP	16	8	3	1	256	128	0.1	0.05	0.3	-	128	0.005	10
SMD	16	8	2	1	168	336	0.1	0.05	0.3	-	128	0.001	10
SWaT	16	8	1	2	216	432	0.1	0.05	0.4	-	128	0.0005	10

B.4 Technical Evaluation Note

We compute final metrics for imputation and forecasting as weighted averages across batches to account for varying batch sizes during evaluation. This adjustment is necessary because the last batch in an epoch may contain fewer samples than the standard batch size. When computing performance metrics by simply averaging across batches without considering batch sizes, smaller batches receive disproportionate weight in the final metric calculation, leading to biased performance estimates that do not accurately reflect true model performance across the entire dataset. In many older works, researchers addressed this problem by setting the drop_last=True parameter in PyTorch's DataLoader, which discards the final incomplete batch to ensure identical batch sizes. However, this approach wastes data and can be particularly problematic for smaller datasets, where discarding samples reduces available training or evaluation data In recent works, it is more common to solve this problem by setting drop_last=False and computing weighted averages, where each batch's metric contribution is weighted by its actual size, ensuring that the final averaged metric accurately represents performance across all samples in the dataset without discarding any data.

C   Appendix: Extended Analysis

C.1   Interpretable Learned Masks Analysis.

CRAB (Sec. 4.2) introduces a learnable non-boolean mask designed to learn the most dominant cross-channel and time dependencies. The mask learns dominant dependencies because it directly modulates the strength of attention values during training. Specifically, the mask multiplies attention weights element-wise, where higher absolute mask values amplify the corresponding attention relationships while values near zero suppress them. Through gradient-based optimization, the mask automatically discovers which cross-channel and temporal interactions are most informative for the downstream task, effectively learning a data-driven weighting scheme that prioritizes the most predictive dependencies.

Examining the learned mask can therefore provide data-specific insights about these dependency structures, as the mask values directly reflect relationship dominance with higher absolute values indicating stronger learned dependencies. In this section, we explain how to interpret the attention mask as a foundation for further analysis so it can be leveraged for different analytical needs.

Following data processing (Sec. 4.1), the input data is first permuted so that the patch sequence dimension is placed before the channel dimension, then sequence and channel are flattened. This creates an attention mask structure that can be visualized as a grid of squares where each square represents cross-channel relationships between pairs of time steps (refer to Figure 3 for visual representation), with the main diagonal squares capturing cross-channel interactions within the same time step and off-diagonal squares revealing temporal cross-channel dependencies.
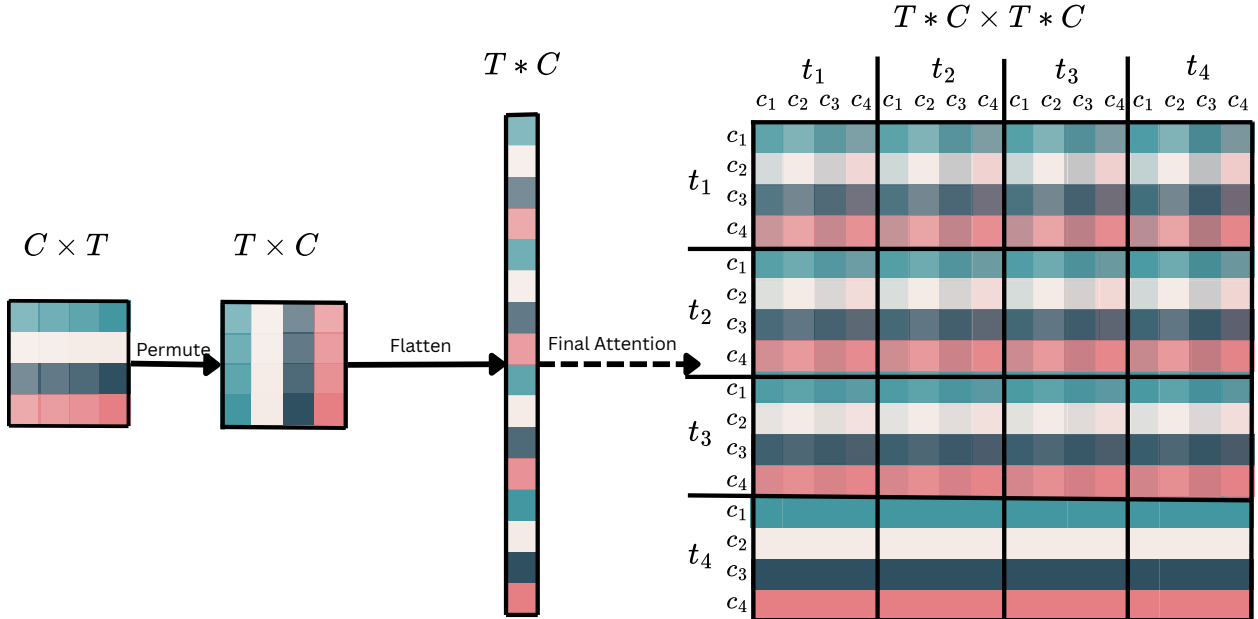
Figure 3: Interpretable Learned Mask Structure: The data permutation step places the patch sequence dimension first, creating an attention mask that can be visualized as a grid of squares where each square represents cross-channel relationships between pairs of time-steps. Note: batch and data dimensions are excluded from this diagram for clarity.

Analysis of Learnable Masks on ETTm1 Dataset   Figure 4 analyzes learnable attention masks trained on the ETTm1 dataset across two forecasting scenarios: 96→96 (top row) and 96→192 (bottom row). Each row displays three visualizations: initial random masks initiated from normal distribution (left), learned patterns after training (middle), and corresponding heatmaps quantifying cross-channel dependency strength (right).

Data Processing and Architecture. The ETTm1 dataset was processed using patches of length 16 with stride 8, generating 12 patches across ETTm1's 7 channels. This configuration produces an 84×84 attention matrix ($12 \times 7 = 84$ dimensions) that captures both temporal and cross-channel relationships.

Heatmap Interpretation. The dependency strength heatmaps are derived from the trained masks by averaging the absolute values within each cross-channel grid. Since masks are applied to attention weights, higher absolute mask values correspond to more dominant dependencies, with darker red regions in the heatmap indicating stronger cross-channel relationships between specific time steps.

Key Findings. The trained masks exhibit several notable patterns. First, they develop structured grid formations that align precisely with the 12-patch architecture, suggesting the model learns systematic cross-channel dependencies. By examining the heatmaps from both configurations, we observe a high density of dominant dependencies along the main diagonal. This diagonal concentration indicates that the model learns strong self-attention patterns where each time step primarily attends to itself and its immediate temporal neighbors. Such patterns suggest that the most informative relationships for forecasting are local temporal dependencies, where recent observations carry the strongest predictive power for future values. This finding aligns with the intuitive understanding that in time series analysis, temporally proximate data points are typically more relevant than distant historical information.
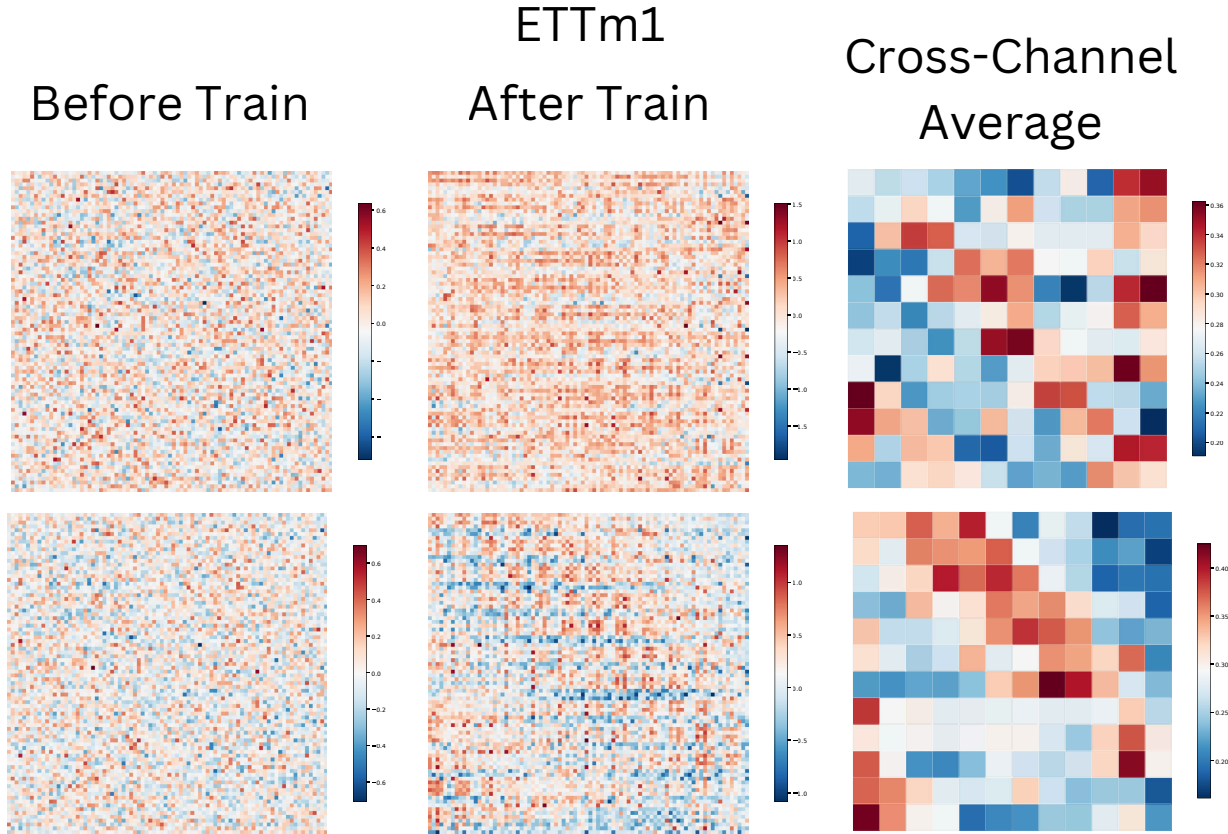
Figure 4: Analysis of learnable attention masks on ETTm1 dataset. Top row: 96→96 forecasting; bottom row: 96→192 forecasting. Left column: initial random masks; middle column: learned structured patterns after training; right column: heatmaps of cross-channel dependency strength derived from trained masks. The heatmaps visualize the strength of cross-channel dependencies between time points, with darker red regions indicating stronger relationships.

D Appendix: Full Results

D.1 Ablation Study: Complete Analysis

We conduct a systematic ablation study with six configurations to isolate the contribution of each architectural component in **XCTFormer**. All variants maintain identical data processing (patch length/stride), training procedures, and model parameters, except for the specific component being modified.

Configuration Details

1. **Full XCTFormer (Baseline)**: Complete architecture including CRAB module, learnable non-boolean mask, DeCoP, cross-time and cross-channel attention, and our proposed attention activation function.

2. **W/o Learnable Mask**: Removes the learnable mask component. Attention masks are not converted to positive values and no element-wise multiplication is applied. The CRAB module remains unchanged otherwise.

3. **Standard Softmax Activation**: Replaces our proposed activation function with standard Transformer softmax while preserving CRAB and the learnable mask. Note that our `attention_dropout` rate parameter is replaced with the standard `dropout` argument commonly used in related work for fair comparison.

4. **Vanilla Transformer**: Substitutes CRAB (and DeCoP) with standard attention blocks following Vaswani et al. (2017).

5. **Sequence Modeling Only**: Retains only temporal self-attention within each channel, disabling cross-channel modeling (channel-independent processing). This configuration tests the necessity of modeling cross-channel relationships, mirroring approaches like PatchTST (Nie et al., 2023).

6. **Channel Modeling Only**: Preserves only cross-channel attention at each time step while removing temporal self-attention. This configuration tests the necessity of modeling temporal relationships, similar to designs that emphasize cross-variable mixing like iTransformer (Liu et al., 2024).

Full Ablation Study Results Complete ablation study results for each time-series task are presented in Tables 10, 11, and 12. For long-term forecasting and imputation tasks, the results shown for each dataset represent averages across all prediction horizons and mask ratios, respectively.

Table 10: Ablation study results for Long-term Forecasting across different datasets, evaluated with different XCTFormer variations.

	ETTh1		ETTh2		ETTm1		ETTm2		Electricity		traffic		weather		XCTFormer vs Others
	MSE	MAE	MSE	MAE	MSE	MAE	MSE	MAE	MSE	MAE	MSE	MAE	MSE	MAE	(%)
XCTFormer (Original)	0.450	<u>0.436</u>	**0.369**	**0.396**	**0.369**	**0.392**	**0.270**	**0.319**	**0.166**	**0.263**	**0.435**	<u>0.287</u>	**0.237**	**0.267**	-
W/o mask	0.453	0.440	0.383	0.405	0.379	0.394	0.282	0.326	0.180	0.273	**0.435**	<u>0.287</u>	0.256	0.280	+2.5%
Original softmax activation	**0.443**	**0.435**	0.390	0.409	0.410	0.413	0.280	0.326	0.224	0.317	0.520	0.368	0.247	0.278	+8.0%
Vanilla transformer	0.452	0.439	0.397	0.412	0.385	0.398	0.285	0.330	0.224	0.317	0.520	0.368	0.263	0.284	+8.3%
Sequence modeling	<u>0.449</u>	0.436	<u>0.380</u>	<u>0.404</u>	<u>0.375</u>	<u>0.393</u>	0.281	0.327	0.195	0.280	0.450	**0.284**	0.256	0.279	+2.8%
Channel modeling	0.461	0.450	0.388	0.409	0.378	0.393	<u>0.278</u>	<u>0.321</u>	**0.166**	**0.263**	0.476	0.329	<u>0.239</u>	<u>0.269</u>	+3.4%

D.2 Robustness Across Random Seeds: Complete Analysis

Coefficient of Variation (CV) for a Single Metric We quantify run to run stability using the coefficient of variation, a unitless measure of dispersion relative to the mean (Reed et al., 2002). For a metric with mean μ and standard deviation σ across five seeds (2021 to 2025), we compute:

$$\text{CV}(\%) = 100 \cdot \frac{\sigma}{|\mu|}.$$

Table 11: Ablation study results for Imputation across different datasets, evaluated with different XCTFormer variations.

	ETTm1		ETTm2		ETTh1		ETTh2		weather		Electricity		XCTFormer vs Others
	MSE	MAE	MSE	MAE	MSE	MAE	MSE	MAE	MSE	MAE	MSE	MAE	(%)
XCTFormer (Original)	**0.029**	**0.113**	**0.024**	**0.092**	<u>0.087</u>	0.201	**0.046**	**0.144**	**0.031**	0.050	**0.046**	<u>0.141</u>	-
W/o mask	0.041	0.132	0.029	0.100	0.092	0.206	0.064	0.169	<u>0.031</u>	<u>0.047</u>	**0.046**	<u>0.141</u>	+8.5%
Original softmax activation	<u>0.032</u>	<u>0.117</u>	<u>0.027</u>	<u>0.099</u>	**0.078**	**0.192**	0.065	0.178	0.040	0.075	0.077	0.196	+14.7%
Vanilla transformer	0.043	0.137	0.033	0.113	0.094	0.208	0.079	0.193	0.031	0.048	0.077	0.196	+19.9%
Sequence modeling	0.040	0.130	0.029	0.101	0.089	<u>0.201</u>	0.081	<u>0.166</u>	**0.031**	**0.047**	**0.046**	**0.139**	+8.7%
Channel modeling	0.065	0.174	0.044	0.136	0.203	0.305	<u>0.060</u>	0.167	0.041	0.072	<u>0.075</u>	0.191	+34.6%

Table 12: Ablation study results for Anomaly Detection across different datasets, evaluated with different XCTFormer variations.

	PSM	SWaT	MSL	SMAP	SMD	XCTFormer vs Others
	F-Score	F-Score	F-Score	F-Score	F-Score	(%)
XCTFormer (Original)	**95.3**	92.6	<u>79.0</u>	**86.7**	<u>84.2</u>	-
W/o mask	95.3	88.2	72.3	66.7	83.0	+8.0%
Original softmax activation	95.3	90.2	69.0	<u>68.6</u>	**84.3**	+7.5%
Vanilla transformer	<u>95.3</u>	<u>93.1</u>	71.8	66.9	83.2	+6.7%
Sequence modeling	95.3	**93.5**	**79.4**	67.5	83.9	+4.4%
Channel modeling	92.9	92.5	76.9	66.5	82.8	+6.4%

The coefficient of variation tells us how much results vary around their mean *relative* to the mean itself. Since CV is unitless, it enables comparison across datasets and metrics: smaller values indicate greater stability, while larger values indicate greater variability.

Confidence score mapping For intuitive interpretation, we report a complementary confidence score:

$$\text{Conf}(\%) = 100 - \text{CV}(\%).$$

This confidence score inverts the scale so that lower variability corresponds to higher confidence. For example, if CV = 3.2%, then Conf = 96.8%, indicating that repeated runs with identical setups produce very similar results.

Full Seed Analysis Results To enhance readability, we include only the averaged analysis table for all time-series tasks in the main paper, while the complete results are provided in Tables 13, 14 and 15. The confidence score presented for each dataset represents the average confidence score across all of its metrics.

Table 13: Standard deviation for XCTFormer on forecasting datasets, evaluated across five seeds (2021-2025). Results averaged over the four prediction lengths $\{96, 192, 336, 720\}$.

Model	CausalityFormer (Ours)		Confidence Score
Dataset	MSE	MAE	Score %
ETTh1	0.449 ± 0.002	0.436 ± 0.001	99.7%
ETTh2	0.374 ± 0.007	0.399 ± 0.004	98.5%
ETTm1	0.371 ± 0.003	0.393 ± 0.002	99.3%
ETTm2	0.271 ± 0.001	0.319 ± 0.001	99.6%
Electricity	0.176 ± 0.007	0.270 ± 0.007	96.6%
traffic	0.435 ± 0.001	0.287 ± 0.001	99.7%
weather	0.237 ± 0.001	$0.267 \pm 9.81e - 04$	99.5%

Table 14: Results of the imputation task across datasets, evaluated across five seeds (2021-2025). We randomly mask $\{12.5\%, 25\%, 37.5\%, 50\%\}$ of the time points; the final results are averaged across these four masking ratios.

Model	CausalityFormer (Ours)		Confidence Score
Dataset	MSE	MAE	Score %
ETTh1	0.090 ± 0.002	0.204 ± 0.003	98.0 %
ETTh2	0.052 ± 0.013	0.153 ± 0.020	80.9 %
ETTm1	0.031 ± 0.004	0.116 ± 0.007	90.2 %
ETTm2	0.026 ± 0.003	0.097 ± 0.007	90.8 %
ETT(Avg)	0.049 ± 0.006	0.143 ± 0.009	91.1 %
Electricity	0.051 ± 0.008	0.149 ± 0.014	87.6 %
weather	$0.031 \pm 5.26e - 04$	0.049 ± 0.002	96.9 %

Table 15: Results for the anomaly detection task (P, R, and F1 are precision, recall, and F1-score in %), evaluated across five seeds (2021-2025).

Model	CausalityFormer (Ours)			Confidence Score
Dataset	Precision	Recall	F1	Score %
MSL	87.84 ± 1.73	66.66 ± 3.92	75.77 ± 3.18	96.0%
PSM	98.31 ± 0.09	93.05 ± 0.57	95.61 ± 0.34	99.6%
SMAP	91.81 ± 1.78	64.59 ± 14.53	75.22 ± 10.43	87.2%
SMD	87.01 ± 0.25	81.99 ± 1.15	84.42 ± 0.69	99.2%
SWaT	91.94 ± 0.49	92.01 ± 1.32	91.98 ± 0.86	99.0%

D.3 Long-Term Forecasting Results

To improve readability, we present only the averaged table for long-term forecasting in the main paper and provide the full results here.

Table 16: Long-term forecasting results comparison across multiple datasets and horizons. We compare extensive competitive models under different prediction lengths. *Avg* is averaged from all four prediction lengths, that $\{96, 192, 336, 720\}$.

Models		XCTFormer (Ours)		MTLinear[1] (AISTATS 2025)		Leddam (ICML 2024)		TimeMixer (ICLR 2024)		iTransformer (ICLR 2024)		PatchTST (ICLR 2023)		Crossformer (ICLR 2023)		TiDE (TMLR 2023)		TimesNet (ICLR 2023)		DLinear (AAAI 2023)		SCINet (NeurIPS 2022)		FEDformer (ICML 2022)		Autoformer (NeurIPS 2021)	
Metric		MSE	MAE	MSE	MAE	MSE	MAE	MSE	MAE	MSE	MAE	MSE	MAE	MSE	MAE	MSE	MAE	MSE	MAE	MSE	MAE	MSE	MAE	MSE	MAE	MSE	MAE
ETTm1	96	0.302	0.350	0.337	0.363	0.319	0.359	0.320	0.357	0.334	0.368	0.352	0.374	0.404	0.426	0.364	0.387	0.338	0.375	0.346	0.374	0.418	0.438	0.379	0.419	0.505	0.475
ETTm1	192	0.354	0.382	0.379	0.387	0.369	0.383	0.361	0.381	0.390	0.393	0.374	0.387	0.450	0.451	0.398	0.404	0.374	0.387	0.382	0.391	0.439	0.450	0.426	0.441	0.553	0.496
ETTm1	336	0.385	0.404	0.412	0.409	0.394	0.402	0.390	0.404	0.426	0.420	0.421	0.414	0.532	0.515	0.428	0.425	0.410	0.411	0.415	0.415	0.490	0.485	0.445	0.459	0.621	0.537
ETTm1	720	0.435	0.433	0.468	0.443	0.460	0.442	0.454	0.441	0.491	0.459	0.462	0.449	0.666	0.589	0.487	0.461	0.478	0.450	0.473	0.451	0.595	0.550	0.543	0.490	0.671	0.561
ETTm1	Avg	0.369	0.392	0.399	0.401	0.385	0.397	0.381	0.396	0.410	0.410	0.402	0.406	0.513	0.495	0.419	0.419	0.400	0.406	0.404	0.408	0.485	0.481	0.448	0.452	0.588	0.517
ETTm2	96	0.168	0.252	0.175	0.254	0.176	0.257	0.175	0.258	0.180	0.264	0.183	0.270	0.287	0.366	0.207	0.305	0.187	0.267	0.193	0.293	0.286	0.377	0.203	0.287	0.255	0.339
ETTm2	192	0.232	0.295	0.240	0.296	0.243	0.303	0.237	0.299	0.250	0.309	0.255	0.314	0.414	0.492	0.290	0.364	0.249	0.309	0.284	0.361	0.399	0.445	0.269	0.328	0.281	0.340
ETTm2	336	0.289	0.332	0.301	0.335	0.303	0.341	0.298	0.340	0.311	0.348	0.309	0.347	0.597	0.542	0.377	0.422	0.321	0.351	0.382	0.429	0.637	0.591	0.325	0.366	0.339	0.372
ETTm2	720	0.391	0.395	0.402	0.393	0.400	0.398	0.391	0.396	0.412	0.407	0.412	0.404	1.730	1.042	0.558	0.524	0.408	0.403	0.558	0.525	0.960	0.735	0.421	0.415	0.433	0.432
ETTm2	Avg	0.270	0.319	0.279	0.320	0.280	0.325	0.275	0.323	0.288	0.332	0.290	0.334	0.757	0.611	0.358	0.404	0.291	0.333	0.354	0.402	0.571	0.537	0.304	0.349	0.327	0.371
ETTh1	96	0.389	0.400	0.386	0.393	0.377	0.394	0.375	0.400	0.386	0.405	0.460	0.447	0.423	0.448	0.479	0.464	0.384	0.402	0.397	0.412	0.654	0.599	0.395	0.424	0.449	0.459
ETTh1	192	0.440	0.429	0.439	0.421	0.424	0.422	0.429	0.421	0.441	0.512	0.477	0.429	0.471	0.474	0.525	0.492	0.436	0.429	0.446	0.441	0.719	0.631	0.469	0.470	0.500	0.482
ETTh1	336	0.479	0.447	0.476	0.441	0.459	0.442	0.484	0.458	0.487	0.458	0.546	0.496	0.570	0.546	0.565	0.515	0.491	0.469	0.489	0.467	0.778	0.659	0.530	0.499	0.521	0.496
ETTh1	720	0.490	0.468	0.472	0.460	0.463	0.459	0.498	0.482	0.503	0.491	0.544	0.517	0.653	0.621	0.594	0.558	0.521	0.500	0.513	0.510	0.836	0.699	0.598	0.544	0.514	0.512
ETTh1	Avg	0.450	0.436	0.443	0.429	0.431	0.429	0.447	0.440	0.454	0.467	0.507	0.472	0.529	0.522	0.541	0.507	0.458	0.450	0.461	0.458	0.747	0.647	0.498	0.484	0.496	0.487
ETTh2	96	0.295	0.342	0.288	0.336	0.292	0.343	0.289	0.341	0.297	0.349	0.308	0.355	0.745	0.584	0.400	0.440	0.340	0.374	0.340	0.394	0.707	0.621	0.358	0.397	0.346	0.388
ETTh2	192	0.370	0.393	0.375	0.388	0.367	0.389	0.372	0.392	0.380	0.400	0.393	0.405	0.877	0.656	0.528	0.509	0.402	0.414	0.482	0.479	0.860	0.689	0.429	0.439	0.456	0.452
ETTh2	336	0.402	0.417	0.412	0.423	0.412	0.424	0.386	0.414	0.428	0.432	0.427	0.436	1.043	0.731	0.643	0.571	0.452	0.452	0.591	0.541	1.000	0.744	0.496	0.487	0.482	0.486
ETTh2	720	0.411	0.433	0.418	0.440	0.419	0.438	0.412	0.434	0.427	0.445	0.436	0.450	1.104	0.763	0.874	0.679	0.462	0.468	0.839	0.661	1.249	0.838	0.463	0.474	0.515	0.511
ETTh2	Avg	0.369	0.396	0.373	0.397	0.372	0.398	0.365	0.395	0.383	0.407	0.391	0.411	0.942	0.683	0.611	0.550	0.414	0.427	0.563	0.519	0.954	0.723	0.436	0.449	0.450	0.459
Weather	96	0.153	0.199	0.159	0.211	0.156	0.202	0.163	0.209	0.174	0.214	0.186	0.227	0.195	0.271	0.202	0.261	0.172	0.220	0.195	0.252	0.221	0.306	0.217	0.296	0.266	0.336
Weather	192	0.199	0.242	0.202	0.252	0.207	0.250	0.208	0.250	0.221	0.254	0.234	0.265	0.209	0.277	0.242	0.298	0.219	0.261	0.237	0.295	0.261	0.340	0.276	0.336	0.307	0.367
Weather	336	0.257	0.286	0.259	0.294	0.262	0.291	0.251	0.287	0.278	0.296	0.284	0.301	0.273	0.332	0.287	0.335	0.280	0.306	0.282	0.331	0.309	0.378	0.339	0.380	0.359	0.395
Weather	720	0.339	0.340	0.332	0.346	0.343	0.343	0.339	0.341	0.358	0.347	0.356	0.349	0.379	0.401	0.351	0.386	0.365	0.359	0.345	0.382	0.377	0.427	0.403	0.428	0.419	0.428
Weather	Avg	0.237	0.267	0.238	0.276	0.242	0.272	0.240	0.272	0.258	0.278	0.265	0.285	0.264	0.320	0.270	0.320	0.259	0.286	0.265	0.315	0.292	0.363	0.309	0.360	0.338	0.382
ECL[p]	96	0.138	0.237	0.183	0.265	0.141	0.235	0.153	0.247	0.148	0.240	0.190	0.296	0.219	0.314	0.237	0.329	0.168	0.272	0.210	0.302	0.247	0.345	0.193	0.308	0.201	0.317
ECL[p]	192	0.164	0.261	0.183	0.268	0.159	0.252	0.166	0.256	0.162	0.253	0.199	0.304	0.231	0.322	0.236	0.330	0.184	0.322	0.210	0.305	0.257	0.355	0.201	0.315	0.222	0.334
ECL[p]	336	0.170	0.266	0.196	0.283	0.173	0.268	0.185	0.277	0.178	0.269	0.217	0.319	0.246	0.337	0.249	0.344	0.198	0.300	0.223	0.319	0.269	0.369	0.214	0.329	0.231	0.443
ECL[p]	720	0.190	0.286	0.231	0.317	0.201	0.295	0.225	0.310	0.225	0.317	0.258	0.352	0.280	0.363	0.284	0.373	0.220	0.320	0.258	0.350	0.299	0.390	0.246	0.355	0.254	0.361
ECL[p]	Avg	0.166	0.263	0.198	0.283	0.168	0.263	0.182	0.273	0.178	0.270	0.216	0.318	0.244	0.334	0.252	0.344	0.193	0.304	0.225	0.319	0.268	0.365	0.213	0.327	0.227	0.364
Traffic[p]	96	0.402	0.269	0.647	0.383	0.426	0.276	0.462	0.285	0.395	0.268	0.526	0.347	0.644	0.429	0.805	0.493	0.593	0.321	0.650	0.396	0.788	0.499	0.587	0.366	0.613	0.388
Traffic[p]	192	0.424	0.281	0.594	0.359	0.458	0.289	0.473	0.296	0.417	0.276	0.522	0.332	0.665	0.431	0.756	0.474	0.617	0.336	0.598	0.370	0.789	0.505	0.604	0.373	0.616	0.382
Traffic[p]	336	0.444	0.291	0.601	0.362	0.486	0.297	0.498	0.296	0.433	0.283	0.517	0.334	0.674	0.420	0.762	0.477	0.629	0.336	0.605	0.373	0.797	0.508	0.621	0.383	0.622	0.337
Traffic[p]	720	0.472	0.307	0.640	0.382	0.498	0.313	0.506	0.313	0.467	0.302	0.552	0.352	0.683	0.424	0.719	0.449	0.640	0.350	0.645	0.394	0.841	0.523	0.626	0.382	0.660	0.408
Traffic[p]	Avg	0.435	0.287	0.621	0.372	0.467	0.294	0.485	0.297	0.428	0.282	0.529	0.341	0.667	0.426	0.760	0.473	0.620	0.336	0.625	0.383	0.804	0.509	0.609	0.376	0.628	0.379
1st Count		14	12	2	6	5	4	4	3	4	4	0	0	0	0	0	0	0	0	0	0	0	0	0	0	0	0

[1] Reported MTLinear results reflect the per-dataset best of MTNLinear and MTDLinear (Nochumsohn et al., 2025).
[p] DeCoP was enabled for XCTFormer on this dataset.